EUROPEAN COMMISSION

European Research Area

Long-term Performance of Engineered Barrier Systems PEBS

Contract (grant agreement) number: ***FP7-249681***

DELIVERABLE (D-N°: D2.3-6-1)

Geochemical interactions at the concrete-bentonite interface of column experiments

Author(s):

E. Torres, M.J. Turrero, A. Escribano, P.L. Martín

Date of issue of this report: **16/12/13**

Start date of project: **01/03/10** Duration : **48** Months

Revised	**Approved**
J. Cuevas, R. Fernández	
16/12/2013	

Project co-funded by the European Commission under the Seventh Euratom Framework Programme for Nuclear Research &Training Activities (2007-2011)		
Dissemination Level		
PU	Public	X
RE	Restricted to a group specified by the partners of the PEBS project	
CO	Confidential, only for partners of the PEBS project	

EURATOM

Summary

Concrete could be part of the barrier system and/or be needed during repository construction. Depending upon the design, concrete could be physically in contact with the bentonite, or be sufficiently close that alkaline pore fluid from the cement may interact with the bentonite barrier, affecting its properties.

CIEMAT performed a comprehensive study based on a series of short term experiments in the framework of NF-PRO project in order to provide experimental evidences on the physical, chemical and mineralogical changes during the concrete-compacted bentonite interaction.

Concrete and bentonite samples were analysed by means of XRD, FTIR spectroscopy and SEM-EDS. In addition, in bentonite sections, chemical analysis for cation exchange capacity and soluble salts were performed.

Table of contents

LIST OF FIGURES

LIST OF TABLES

1. INTRODUCTION

A Deep Geological Repository (DGR), based on the concept of multibarriers, is the solution proposed by most countries for the management of High Level Radioactive Waste (HLW). In order to isolate the wastes, a series of barriers are inserted between the wastes and the biosphere.

The Spanish repository design contains concrete to support the access galleries and in the final sealing of access routes. Concrete will be in contact with the clay host rock and the bentonite barriers. A OPC Cement in contact with the bentonite barrier will be a source of alkaline fluids in wet conditions. Concrete (hydrated cement) pore fluids are in quasi-equilibrium with the solid hydrated phases of the matrix [1, 2]. Calcium solubility is principally controlled by portlandite (CH in cement notation; $Ca(OH)_2$). Sulfate and Al solubility is limited by ettringite (AFt: tri- sulfate aluminate phase) or monosulfoaluminate (AFm), Mg contents are controlled by $Mg(OH)_2$ and Al solubility also by hydrated tri-calcium aluminates Hydrogarnets (C_3AH_6). Silicon concentrations are controlled by the solubility of alkali-containing calcium (C)-silicate (S)-Hydrates (C-S-H) gels. Alkaline cement pore water enhances the solubility of many radioactive elements.

The products generated in the concrete/bentonite interface at the repository conditions can diffuse through the porous structure of the bentonite affecting their properties. The experimental studies conducted by CIEMAT during past EU NF-PRO project and going on in the context of EU PEBS project are based on a series of experiments designed to provide experimental evidences on the physical, chemical and mineralogical changes during the concrete-compacted bentonite interaction.

The aim of the work reported here is studying the interaction of the concrete with the bentonite, based on a series of short term experiments (6, 12 and 18 months). The changes in the chemical and physical properties of the bentonite are measured through the analysis of parameters such as: mineralogy, variations in solid and aqueous composition and specific surface area.

The report begins with a general overview of the state of the art in relation with the concrete degradation and bentonite alteration in the EBS and considers experimental and methodological issues. Chapter 2, 3 y 4 presents experimental evidences and discussion related to the geochemical processes occurring at the concrete, the concrete/bentonite interface and the bentonite. The focus of these chapters is to provide as much experimental data as are available from column experiments specifically designed to be dismantled sequentially to understand the short-term evolution of the system. Finally, chapter 5 provides the most important findings

related to the short-term evolution of the EBS and chapter 6 the references cited in the work.

1.1 General overview

1.1.1 Concrete degradation

Concrete as a component of the multi-barrier system in a Deep Geological Repository is widely used due to its physic-chemical characteristics. Concrete barriers limit the contact of water rock with wastes and provide mechanical and chemical stability.

Uncertainties related to the use of cementitious materials in Nuclear Waste Management are focused on the evolution of the hydraulic behaviour at large timescales, its capacity to retain radionuclides, mechanisms of degradation and its performance under unsaturated conditions.

Under saturated conditions, the most frequent concrete degradation phenomena are the dissolution and precipitation processes, microstructural alteration and the evolution of the mechanical and transport properties.

The physic-chemical behaviour of concrete will depend on the inherent characteristics to the type of concrete used, the different scenarios and the chemical environment in service.

Chemical attack due to external contaminants can affect its durability, resistance and stability during its performance.

Water is the most aggressive agent, either directly or as a transport media for contaminants.

Aggregate expansion

Various types of aggregate undergo chemical reactions in concrete, leading to damaging expansive phenomena. The most common are those containing reactive silica, that can react (in the presence of water) with the alkalis in concrete (K_2O and Na_2O, coming principally from cement). The more reactive silica containing minerals are opal, chalcedony, flint (microquartz and chalcedony rock) and strained quartz. Following the alkali-silica reaction (ASR) an expansive gel forms, that creates extensive cracks and damage on structural members. On the surface of concrete pavements the ASR can cause pop-outs, i.e. the expulsion of small cones (up to 3 cm about in diameter) in correspondence of aggregate particles. When some aggregates containing dolomite are used, a dedolomitization reaction occurs where the magnesium carbonate compound reacts with hydroxyl ions and yields magnesium hydroxide and a carbonate ion. The resulting expansion may cause destruction of the material.

Far less common are pop-outs caused by the presence of pyrite, an iron sulfide that generates expansion by forming iron oxide and ettringite. Other reactions and recrystallizations, e.g. hydration of clay minerals in some aggregates, may lead to destructive expansion as well.

Chlorides

Chlorides, particularly calcium chloride, have been used to shorten the setting time of concrete. However, calcium chloride and (to a lesser extent) sodium chloride have been shown to leach calcium hydroxide and cause chemical changes in Portland cement, leading to loss of strength as well as attacking the steel reinforcement present in most concrete.

Sulfates

Degradation of cementitious systems exposed to sulfate salts is the result of sulfate transport through the pore system, chemical reaction with the hydration product phases present, generation of stresses due to the creation of the expansive reaction products, and the mechanical response (typically spalling and cracking) of the bulk material due to these stresses. Each component of this process plays a unique role in the ultimate response of the concrete; change the material properties relevant to any one component and the concrete performance can change dramatically.

Often, it is assumed that the performance of concrete regarding its resistance to external sulfate attack depends on the composition of the cement used.

The deterioration of concrete exposed to sulfate is the result of the penetration of aggressive agents into the concrete and their chemical reaction with the cement matrix. The three main reactions involved are:

- Ettringite formation: conversion of hydrated calcium aluminate to calcium sulfoaluminate,
- Gypsum formation: conversion of the calcium hydroxide to calcium sulfate, and
- Decalcification: decomposition of the hydrated calcium silicates.

These chemical reactions can lead to expansion and cracking of concrete, and/or the loss of strength and elastic properties of concrete. The form and extent of damage to concrete will depend on the sulfate concentration, the type of cations (eg. sodium or magnesium) in the sulfate solution, the pH of the solution and the microstructure of the hardened cement matrix. Some cements are more susceptible to magnesium sulfate than sodium sulfate, the key mechanism is the replacement of calcium in calcium silicate hydrates that form much of the cement matrix. This leads to a loss of

the binding properties. Formation of brucite ($Mg(OH)_2$) and magnesium silicate hydrates is an indication of such attack.

The presence of chloride in soil and groundwater may be beneficial since there is considerable evidence, from seawater studies, that the presence of chloride generally reduces expansion due to sulfate attack. The risk of corrosion of embedded metals in buried concrete in non-aggressive soil is generally lower than in externally exposed concrete. However, high chloride concentrations in the ground may increase the risk of corrosion since chloride ions may permeate the concrete, leading to a depassivation of the metal surface.

Leaching

When water flows through cracks present in concrete, water may dissolve various minerals present in the hardened cement paste or in the aggregates, if the solution is unsaturated with respect to them. Dissolved ions, such as calcium (Ca^{2+}), are leached out and transported in solution some distance. If the physic-chemical conditions prevailing in the seeping water evolve with distance along the water path and water becomes supersaturated with respect to certain minerals, they can further precipitate, making deposits or efflorescences inside the cracks, or at the concrete outer surface. This process can cause the self-healing of fractures in particular conditions.

Carbonation

Carbon dioxide from air can react with the calcium hydroxide in concrete to form calcium carbonate. This process is called carbonation, which is essentially the reversal of the chemical process of calcination of lime taking place in a cement kiln. Carbonation of concrete is a slow and continuous process progressing from the outer surface inward, but slows down with increasing diffusion depth. Carbonation has two effects: it increases mechanical strength of concrete, but it also decreases alkalinity, which is essential for corrosion prevention of the reinforcement steel. Below a pH of 10, the steel's thin layer of surface passivation dissolves and corrosion is promoted. For the latter reason, carbonation is an unwanted process in concrete chemistry.

Decalcification

Distilled water can wash out calcium content in concrete, leaving the concrete in brittle condition. A common source of distilled water can be condensed steam. Distilled water leaches out the calcium better because undistilled water contains a certain amount of calcium already, which hinders $Ca(OH)_2$ dissolution.

Microbial degradation

Ferruginous bacterias and thiobacterias are the most relevant microorganisms to concrete degradation, as their metabolism can lead to the formation of sulphuric acid and sulfates under oxic environments.

1.1.2 Bentonite alteration

Furthermore, concrete degradation generates a diffusive alkaline plume, which can affect the swelling and transport properties of the bentonite, as well as the properties of the adjacent host rock and groundwater. Many studies have been performed in order to study the influence of alkaline media on bentonite. Eberl *et al*. [3] reported that the formation of illite or illite/smectite depends on the KOH solution concentration rather than on temperature and time of reaction [4, 5] Formation of mixed layer phases seems to be an intermediate step in a series of dissolution-precipitation processes, including the formation of zeolite minerals.

Cuevas *et al*. [6] carried out a set of batch (alkaline solution and bentonite (25-200 ºC) and column experiments (granitic and alkaline water-mortar-bentonite, 25-120 ºC) experiments in order to study the influence of alkaline media on FEBEX bentonite. The main phases identified in the alkaline reaction of FEBEX bentonite are phillipsite, Mg-clays, analcime, tobermorite and C-S-H gels. The formation of a new smectitic tri-octahedral phase was confirmed, as well.

The ECOCLAY project [7] comprised batch leaching tests with bentonite mixed with four synthetic cement porewater solutions and determination of chemical and microstructural changes at the cement/bentonite interface. Also, tests were made by compaction of MX-80 in a cell to 1.4 and 1.6 g/cm^3 dry density with subsequent drilling of a hole in the bentonite and filling it with fresh cement paste. This closed system was examined after 3 to 12 months with respect to chemical and microstructural changes. In a third test series, a hardened cement disc was placed in contact with bentonite and the system percolated by granitic water. The quantity of dissolved smectite was found to depend on the water content. The average amount of dissolved smectite was found to be 12 g of smectite per liter of pore solution, i.e. 1.2% under the closed conditions that prevailed.

Theorical considerations [8, 9] have indicated that zeolites like phillipsite and analcime should be reaction products and this has also been verified by tests showing that they can be formed in a few months in batch tests with KOH/NaOH/$Ca(OH)_2$ at 90 ºC and after several months at lower temperatures [7]. Interstratified smectite/illite formed when the solution contained much K^+. Uptake of Mg^{2+} in the montmorillonite crystal lattice yielded the smectite species saponite.

The most important conclusions from these earlier studies were:

- High alkali cement degrades quicker than low alkali cement. The latter deteriorates by destruction of the C-A-H gel.
- Dissolved elements and water migrate from the fresh cement paste to the bentonite in the first few hours.
- The cement paste is dehydrated and its voids become wider; water moves from the bentonite to the dense cement matrix.
- The dense paste fissures.
- pH=12.6 seems to be the threshold value for significant changes of the smectite component.
- Ca migrates from the cement to the clay causing ion exchange and change in the microstructure of the clay by coagulating softer parts.

Water-induced alteration of concrete generates alkali-rich high-pH (12.5 - 13.6) solutions [10, 11]. Their release to the surrounding media has been modelled [12-16]. Such models show that solution composition is first controlled by the release of NaOH and KOH leading to very high solution pH (>13). In a second step, the solution composition is controlled by portlandite ($Ca(OH)_2$ – pH 12), and finally by calcium-silicate-hydrates (C-S-H) phases (pH 9-10).

As a consequence, numerous investigations have been conducted on the stability of clays in such high pH conditions [3-5, 17-25]. These studies consistently indicate that the clay minerals described in the Callovo-Oxfordian formation of the MHM site (smectite, illite and mixed-layer illite-smectite [26, 27]) would react when in contact with high-pH alkali-rich solutions. For example, high-pH experimental investigations on smectite-type minerals indicated a fast montmorillonite-to-beideillite transformation [28].

The extent and nature of alkaline alteration can change form batch reactions (high water to solid ratios) to experiments including compacted bentonite [29-32]. It has been observed that hyperalkaline fluids (Na–OH type solutions, pH ≥ 13) that percolate through a compacted bentonite column by advection at temperatures in the range 50–170 °C are able to partially dissolve Mt (Nakayama et al., 2004), thereby increasing the connected macroporosity (large pores that occupy the space between coarse nonclayparticles and aggregates of clay minerals), and thus creating preferential pathways for fluid transport through the bentonite (Fernández et al., 2006; 2013). This process is temperature- and clay density-dependent. The increase in temperature is directly related to a decrease in viscosity that favors fluid flow. However, increased

clay density (dry densities above 1.5 g/cm^3) critically reduced the mineralogical altered thickness to < 5 mm, and prevented zeolite formation by dissolution–precipitation reactions at the pore spaces (Fernández et al., 2012). By contrast, alkaline fluids (Ca–OH type solutions; pH ~12.5) reacted differently with bentonite. In the range of previously studied temperatures (25–120 °C), the reaction was controlled by cementation phenomena and pore clogging at the cement/bentonite interface, while cation exchange processes were detected beyond the mineralogical alteration zone. Moreover, negligible smectite dissolution was observed under these conditions (Fernández et al., 2006).

1.2 Experimental set-up

1.2.1 Materials

Bentonite

The tests have been performed with a bentonite (FEBEX) from the Cortijo de Archidona deposit (Almería, Spain). The conditioning of the bentonite prior its use in the laboratory is detailed in [33]. It's main characteristics are detailed in Villar [34] and summarized as follow.

The bentonite has a content of dioctahedral smectite of the montmorillonite type close to 92%, as determined by X-ray diffraction. Besides, it contains variable quantities of quartz (2 ± 1%), plagioclase (2 ± 1%), cristobalite (2 ± 1%) and traces of potassium feldspar, calcite and trydimite. The cation exchange capacity is of 79 ±2 meq/100g using the Cu-triethylenetetramine method (102 meq/100 g when the NH_4AcO method is used). The exchangeable cations are Ca (38%), Mg (28%), Na (23%) and K (2%). The water content of the clay at laboratory conditions is about 13.7 ± 1.3%.

Blocks of FEBEX bentonite were compacted with its hygroscopic water content (14%) at a nominal dry density of 1.65 g/cm^3 to be placed inside the cells designed for the experiments (see section 1.2.2).

Concrete

Cement used in the tests is an Ordinary Portland Cement CEM-I-SR. Chemical composition is shown in Table I.

Table I. Chemical composition of the CEM I 42.5 R/SR cement [35].

Chemical composition (%)	SiO_2	Al_2O_3	Fe_2O_3	CaO (total)	MgO	SO_3	Na_2O	K_2O	CaO (free)
CEM-I-SR	19.6	4.43	4.27	65.6	0.95	3.29	0.11	0.28	1.92

1.2.2 Experimental Set-up

The tests were carried out in hermetic cylindrical cells (10.1 cm high, 7 cm diameter). The body of the cell is made out of Teflon, although an external steel cylinder prevents its deformation swelling. A plane heater constitutes the bottom of the cell and on the top of the cell a chamber allows the circulation of water at a controlled temperature (around 22 ^{o}C), lower than that of the heater (100 ^{o}C), so a gradient of a temperature is established. A hydration channel crosses the upper chamber and allows the hydration of the sample through a stainless steel sinter. Water is injected under a pressure of 12 bars. The clay, with its water content at equilibrium with the laboratory conditions, is uniaxially compacted outside the cell to a dry density of 1.65 g/cm^3. The cells are inside a methacrylate chamber, under vacuum, to prevent oxidation.

Six medium cells were assembled at a time (Figure 1 and Figure 2) starting operation in March 2006. In them, a concrete slab was placed on the top of the compacted bentonite block. For hydration, a saline solution, whose composition is described in Table II, was used.

In the context of NF-PRO project, three cells were dismantled after 6, 12 and 18 months (Figure 3). These cells are the objective of the present report. The fourth and fifth were dismantled in the framework of the PEBS project after 54 months (results were included in the PEBS Deliverable 2.3-3-1 distributed on October 2011) and 80 months of operation (results will be reported in PEBS Deliverable 2.3-3-3 by the end of 2013). A joint report reporting the whole picture on the evolution of the EBS will be presented as final report of the PEBS project. The sixth cell will keep on working at least for 2 years more.

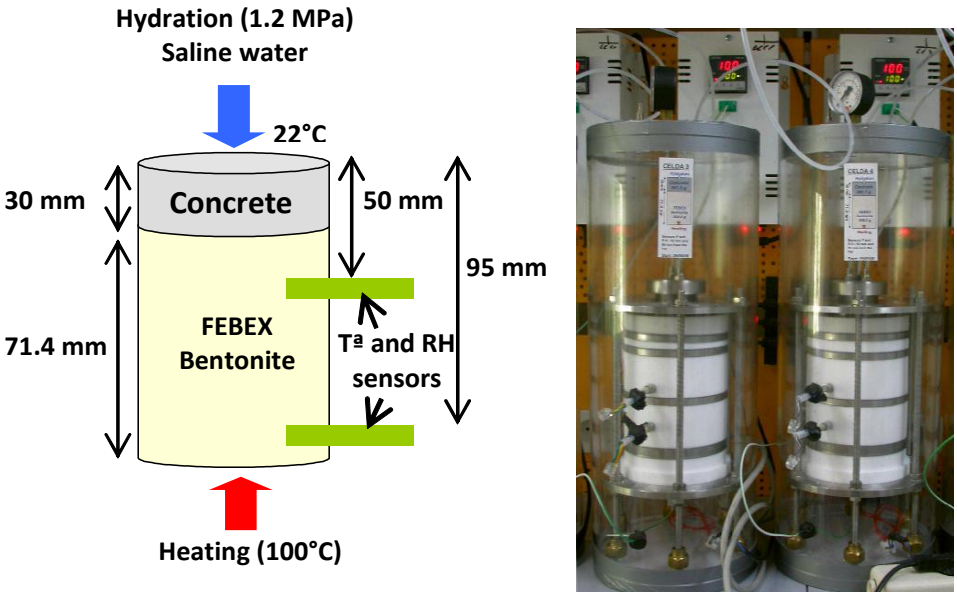

Figure 1. Scheme of one of the cells used in the tests.

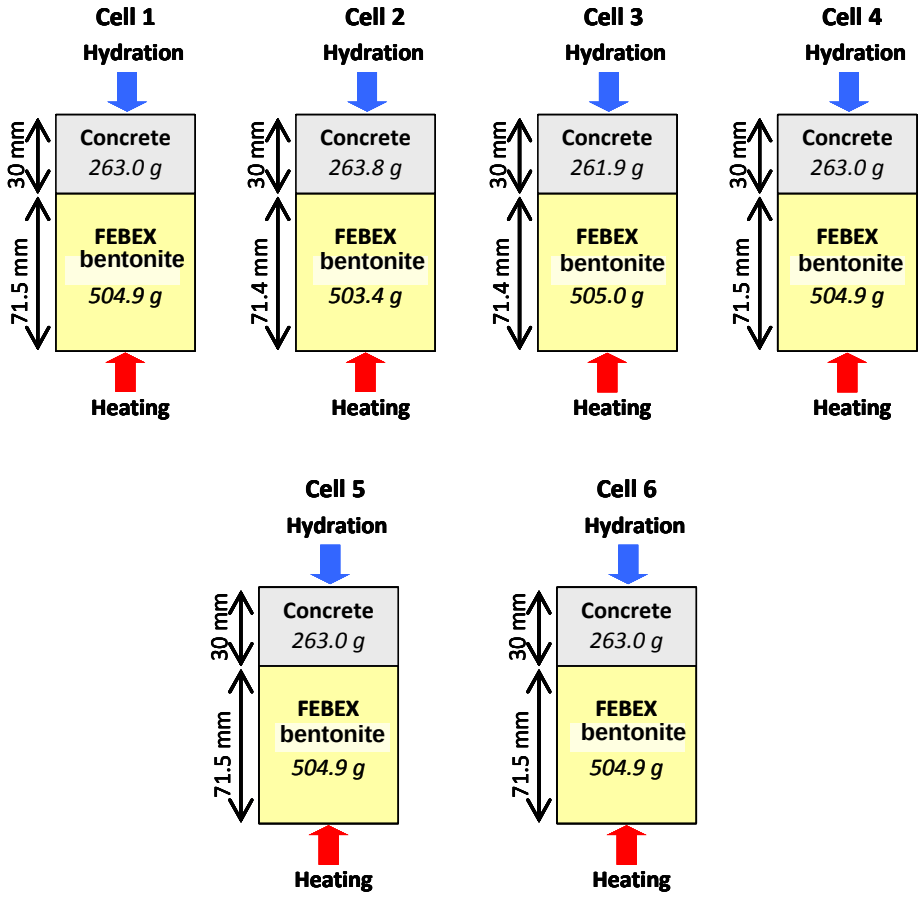

Figure 2. Characteristics and materials in each of the cells assembled.

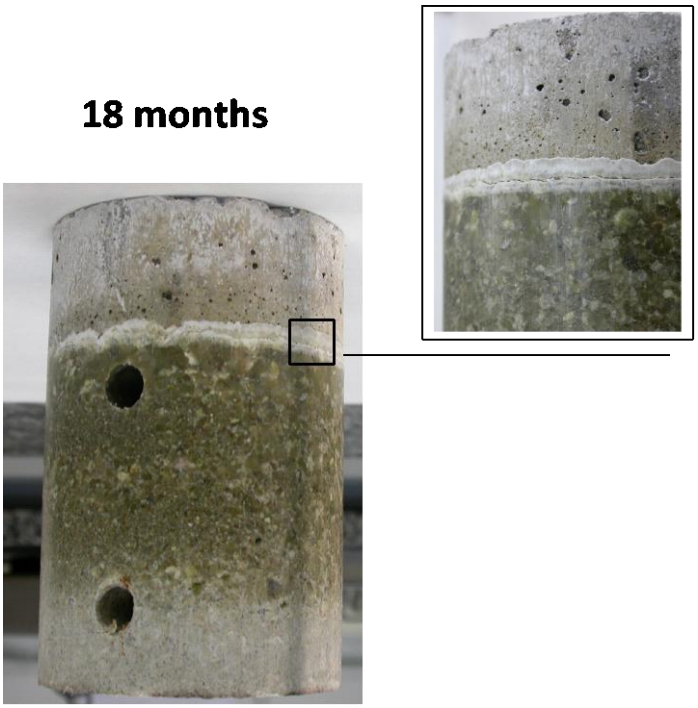

Figure 3. Photographs of the compacted bentonite block and the concrete slab after the dismantling of the 12 and 18-month tests

Two sensors were installed in each cell to monitor the evolution of water content and temperature with time. Sensors were located at 50 and 95 mm from the top of the cell, at the hydration zone and the interface, respectively.

Table II. Chemical composition of the saline solution used for the hydration of the concrete/bentonite cells.

Chemical species	Concentration (M)
Fe	1.1 E-05
Na	1.3 E-01
K	8.2 E-04
Ca	1.1E-02
Mg	8.2E-02
Si	2.7E-04
SO_4^{2-}	7.0E-02
Cl^-	2.3E-02
HCO_3^-	1.8E-03
pH = 7.54 pE = -3.16 log P CO_2 = -2.65	

During the dismantling of the cells, special care was taken to avoid disturbances at the interfaces and to have accurate measurements of the final water content. The blocks

were divided into 3 different sections apart from the samples collected from the concrete/bentonite interaction (Figure 4).

Figure 4. Sampling of the compacted bentonite block from the dismantled cells.

Methods

Two types of samples were collected and analyzed:

1. The precipitates found at the concrete/bentonite interface and some millimetres far away from interface.

2. Bentonite samples at different distances from the interface, named sections 1, 2 and 3 (Figure 4). The samples collected were analyzed by using different techniques.

X-ray diffraction (XRD) and Fourier Transform-Infrared (FTIR) analysis were carried out on the precipitates collected from the concrete bentonite interface.

The XRD equipment used is a Phillips Xpert-MPD diffractometer and the FTIR spectroscope used is a Nicolet 4700 in the range of 4000 to 400 cm^{-1}. XRD patterns of the bentonite samples were obtained on the total sample, ethylene glycol (EG)-saturated and calcined specimens. The morphology and chemical composition of the samples were determined by scanning electron microscopy (SEM) and Energy-dispersive X-ray spectroscopy (EDS) using a JEOL JSM 6400.

Specific surface was measured by means of gas adsorption methods (N_2-BET measures). A Gemini V MICROMERITICS porosimeter was used.

Cation exchange capacity (Cu-triethylenetetramine method) [36], and exchangeable cations ($CsNO_3$ method) [37] analysis were also performed.

2. CONCRETE DEGRADATION

2.1 Introduction

2.1.1 Durability of CEM I 42.5 R/SR

When concrete is exposed to weathering and subsurface environmental conditions, its underlying microstructure can be attacked by a variety of aggressive agents; for example, rainwater and groundwater. The knowledge of concrete resistance to long-term water aggression is necessary for predictions of their performance in different environments. This study aims to analyse the effects of leaching on the microstructure of Portland cements binders.

Calcium silicate hydrate (C-S-H) gel, together with portlandite ($Ca(OH)_2$) and alkalis, dominate the chemical properties of the aqueous phase in Portland cement pastes, and account for its high pH and calcium solubility. The pH of their pore solution is initially greater than 13, as a result of the dissolution of sodium and potassium hydroxides from the cement producing a highly alkaline condition in the groundwater in contact with these materials. This hyperalkaline stage is a short-term stage and, later, when these hydroxides has been removed, the pH would be expected to decrease to around 12.5 and would be controlled by the dissolution of other constituent minerals such as portlandite and C-S-H phases.

C-S-H gels are the main constituents of the hydrated Portland cement systems, characterized by a poor crystalline structure with a variable composition [38, 39]. The CaO/SiO_2 (Ca/Si) ratio and the concentration of calcium control the type of C-S-H gel [40]. The stoichiometry of most of the C-S-H gels has been identified in the range of $0.66<Ca/Si<2$ [40-46]. Various structures of C-S-H gel have been proposed, but Taylor [38] gave the most accepted one, i.e., C-S-H (I) and C-S-H (II), which are similar to tobermorite and jennite, respectively. According to Taylor (1), for Ca/Si = 0.66, the structure of the C-S-H gel presents some analogy with tobermorite, a Th-Oc-Th structure (Th: tetrahedral; Oc: Octahedral), with silicate tetrahedral sheets of SiO_2 linear chains associated to an octahedral sheet of CaO [47, 48], but with some defects [49-52]. The chain length is assumed infinite. The silicate chains are constituted of dimmers ($Si(Q^2)$) connected by bridging tetrahedron ($Si(Q^{2p})$) [38]. Silicate tetrahedrons ($Si(Q^{2p})$) are balanced by H^+. As in the smectite structure, aluminium may substitute silicon in the tetrahedral chains [48, 49]. When the Ca/Si ratio increases from 0.66 up to 1, H^+ is substituted by calcium in the interlayer space. The shortening of the silicate chains arises from higher calcium content [53, 54]. From Ca/Si = 1.65 and about $[Ca^{2+}]$= 22 mM/l, $Ca(OH)_2$ precipitates in equilibrium with the C-S-H gel. For this ratio, the structure of the C-S-H is depicted only by silicate dimmers, because of the silica bridging tetrahedral ($Si(Q^{2p})$) are unstable [55].

According to literature [38], the mineral hydrates, which may be reasonably expected to form a complete hydration of ordinary Portland cement at 25ºC, are C-S-H gel with Ca/Si = 1.8 (jennite type), portlandite, ettrigite AF_t ($3CaO{\cdot}Al_2O_3{\cdot}3CaSO_4{\cdot}32H_2O$), Al monosulfate AF_m ($3CaO{\cdot}Al_2O_3{\cdot}CaSO_4{\cdot}12H_2O$) and M_4AH_{10} ($Mg_4Al_2O_{17}H_{20}$), being aluminium the major element after calcium and silicon, in most cement compositions. Decalcification of cement paste is closely associated with leaching; some authors have indicated that, for cement based materials, decalcification of C-S-H gels proceeds until a constant value of Ca/Si ratio in the solid is reached [56, 57]. As in clays, aluminium in C-S-H could substitute into either the octahedral calcium sites of the cationic CaO plane of the tetrahedral silicon sites.

Sulfate-resistant Portland cement (CEM I 42.5 R/SR) is used in El Cabril facility for the construction of the containers and the disposal structures. According to De la Cruz *et al*. [58], this type of cement is optimal for the construction of on-surface and underground disposal vaults, due to its low content of C_3A (tricalcium aluminates).

Due to its chemical resistance and the previous experience gained from the characterization of concrete structures used in El Cabril, CEM I 42.5 R/SR was chosen for the construction of the seal and for supporting the galleries.

To produce this cement, iron oxide is added to the raw feed to the kiln, which results in the production of a material low in tricalcium aluminate (C_3A). This is the compound that reacts with sulfates to potentially result in sulfate attack, which may lead to the disintegration of the hardened mortar. The increased iron oxide content gives sulfate-resisting Portland cement, a darker colour than plain Portland cement. Sulfate resisting Portland cement is often ground finer than CEM I Class (42.5 N) in order to compensate for the reduced early strength caused by its low C_3A content.

Description of CEM I 42.5 R/SR

In Table III, composition of concrete and mortar of the concretes used in El Cabril is given. Table IV provides a detailed chemical composition of cement CEM I 42.5 R/SR.

Table III. Composition of concrete and mortar of concretes used in El Cabril facility [59].

	Concrete	Mortar
Cement I-42.5 R/SR	400	---
Cement IV-B-32.5 SR/BC	---	708.3
Sand (0-2.5 mm)	297	---
Sand (0-5 mm)	614	---
Sand (ASIROSA)	---	1239.84
Aggregate (6-16)	949	---
Superplastifier Melcret 222	4	---
Admixture Rheobuild 1000	---	7
w/c Ratio	0.45	0.37
w/(c+blending agents) Ratio	0.45	---

Table IV. Chemical analysis of CEM I 42.5 R/SR cement [35].

Chemical composition (%)	**SiO_2**	**Al_2O_3**	**Fe_2O_3**	**CaO (total)**	**MgO**	**SO_3**	**Na_2O**	**K_2O**	**CaO (free)**
CEM-I-SR	19.6	4.43	4.27	65.6	0.95	3.29	0.11	0.28	1.92

Table V summarizes the average mineralogical composition of the cement.

Table V. Average mineralogical composition of CEM I 42.5 R/SR cement [59].

Mineral (%)	**CEM I/SR**
C_3S	77.48
C_2S	<1
C_3A	<1
CA	---
C_4AF	13.38

Technical specifications of CEM I 42.5 R/SR cement according to UNE 80.301:96 standard are shown in Table VI.

Table VI. Physic-chemical characteristics of CEM I 42.5 R/SR cement in El Cabril facility.

		Range of values	UNE specifications
Chemical characteristics	Weight loss upon calcination	3.01	5% maximum
	SO_3	3.10	4% maximum
	Insoluble residue	0.01	5% maximum
	Cl^-	0.01	0.1% maximum
Physical characteristics	Start of hardening	105	≥ 60 minutes
	Final of hardening	155	≤ 12 hours
Compression resistance	2 days	26.7	20 N/mm^2 minimum
	8 days	56.9	42.5 N/mm^2 minimum
Additional characteristics of cement kiln	% C_3A	3.53	5% maximum
	%C_3A+C_4AF	16.05	22% maximum

Table VII compiles additional parameters related to concrete durability that were provided by ENRESA.

Table VII. Parameters related to concrete durability and typical values obtained on El Cabril concrete [59].

Parameters	***Typical mean values***
Compression strength (MPa)	61.13
Porosity (% in volume)	7.25
Density (g/cm^3)	2.31
Coefficient of water absorption ($kg/m^2s^{0.5}$)	1.83E-3
Coefficient of resistance to water penetration (s/m^2)	6.32E+8
Oxygen permeability (m^2)	11.18E-18

2.2 Results

In this section, a compilation of the most relevant results obtained during the characterization of the concrete blocks will be displayed.

Thermogravimetric, FTIR, XRD and SEM-EDS analyses were conducted on the samples collected from the concrete blocks immediately after the dismantling of the cells. This report will be focused on the characterization of the concrete blocks from the 6, 12 and the 18 month-tests.

Due to the high concentration of sulfate in the hydrating solution, the formation of sulfate-bearing phases was expected. Special attention was paid to the sulfate attack and the degradation of concrete because of the expansion of ettringite.

2.2.1 Thermogravimetric analysis

Thermogravimetric analyses were conducted on the concrete samples immediately after the dismantling of the 6, 12 and 18-month test. InFigure 5 to

Figure 7, the corresponding thermogravimetric analyses are displayed.

The weight loss peak around 100 ºC is induced by hygroscopic water. Zone between 100 and approximately 200ºC is attributed to hydration of C-S-H gel. The step at 425-550 ºC is due primarily to decomposition of portlandite. The loss below the portlandite step is due to decomposition of C-S-H and the hydrated aluminate phases, but in this zone, cement pastes show only slight indications of steps. Carbonates show distinctive decomposition peaks at the temperature range of 625-875 ºC.

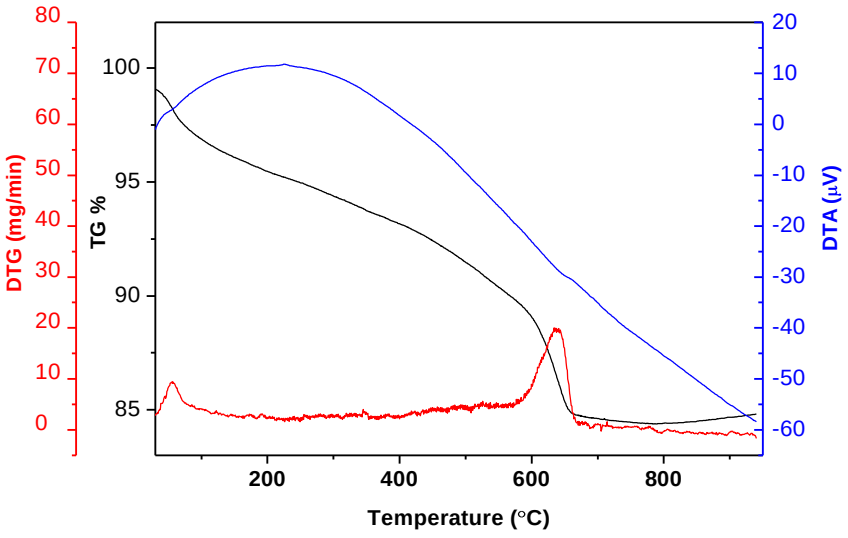

Figure 5. TGA/DTA diagrams recorded for concrete collected from the 6-month test.

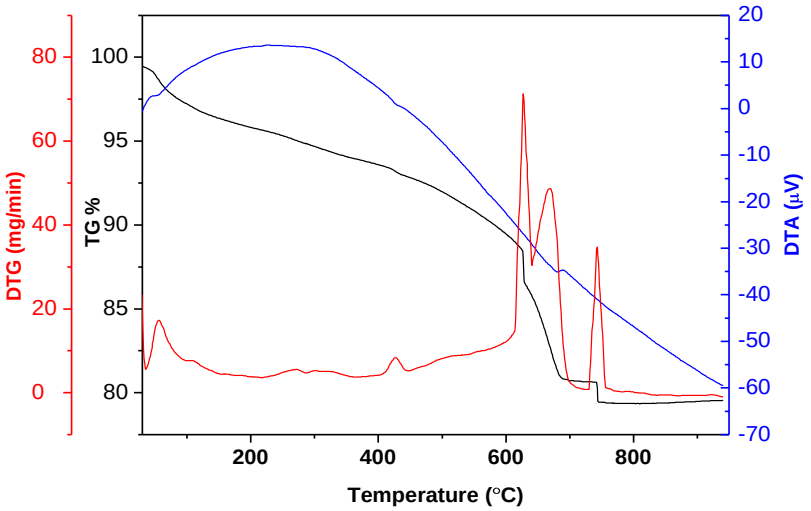

Figure 6. TGA/DTA diagrams recorded for concrete collected from the 12-month test.

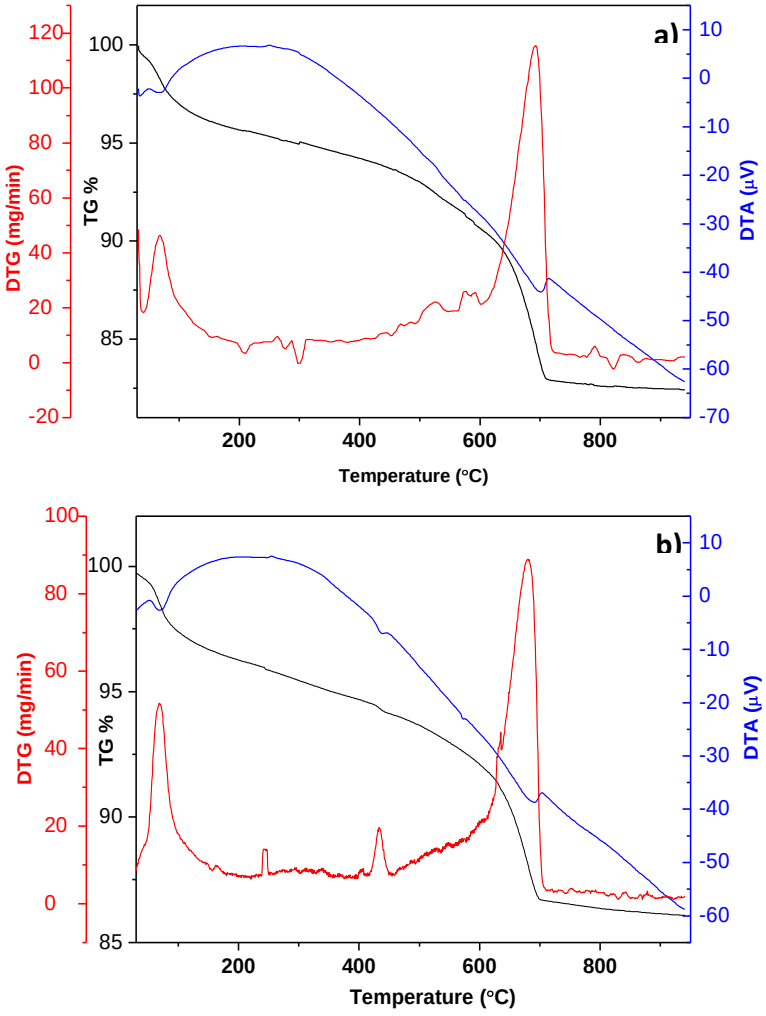

Figure 7. TGA/DTA diagrams recorded for concrete collected from the 18-month test at: a) the hydration zone; b) the concrete/bentonite interface.

DTG diagrams confirmed the existence of calcite in all samples, with an increasing amount depending on the duration of the tests. Calcite usually decomposes at 792 ºC, generally in one step. However, when NaCl is present in the samples, calcite decomposition occurs via four stages. After 12 months, the characterization of concrete revealed the formation of halite [60], as the four peaks typical for NaCl were found at 628, 760, 793 and 930ºC. In the cell dismantled after 18 months, two different samples were analyzed: one from the concrete/bentonite (bottom zone) and another one from the hydration zone (upper zone). At the upper zone (hydration zone), carbonation occurred to some extent. At the contact of bentonite with concrete, gypsum precipitation ($CaSO_4 \cdot 2H_2O$) occurred but in a small amount.

The effect of sulfate attack on concrete seems to be negligible in the short-duration tests (6 and 12 months). In the cell dismantled after 18 months, small amounts of gypsum were found in zones close to the contact with bentonite. No sulfate-rich phases, such as ettringite or thaumasite [61], could be distinguished in the diagrams. The existence of gypsum could be a consequence of the oversaturation of concrete porewater with sulfate at the bottom of the concrete block by leaching from upper zones.

2.2.2 X-ray diffraction analysis

Formation of secondary phases due to the interaction of concrete with the saline hydrating solution was observed in all cases.

Carbonation increased clearly with time and is more intense at the hydration surface than in the rest of the block. Formation of C-S-H gels is time-dependent, as well. In the diffraction patterns, diffraction lines corresponding to tobermorite were found in the three tests. Portlandite and brucite were identified in the 18 month-test, both, at the contact with bentonite and the hydration surface.

Phases identified in the tests are summed up in Table VIII.

Table VIII. Identified phases in the XRD patterns recorded for the concrete samples collected from the 6, 12 and 18-month test.

Time	Identified phases						
	Quartz	Calcite	Tobermorite	Feldspar	Portlandite	Gypsum	Brucite
Unaltered	✓	✓					
6 months	✓	✓	✓				
12 months	✓	✓	✓	✓			
18 months	✓	✓	✓		✓	✓	✓

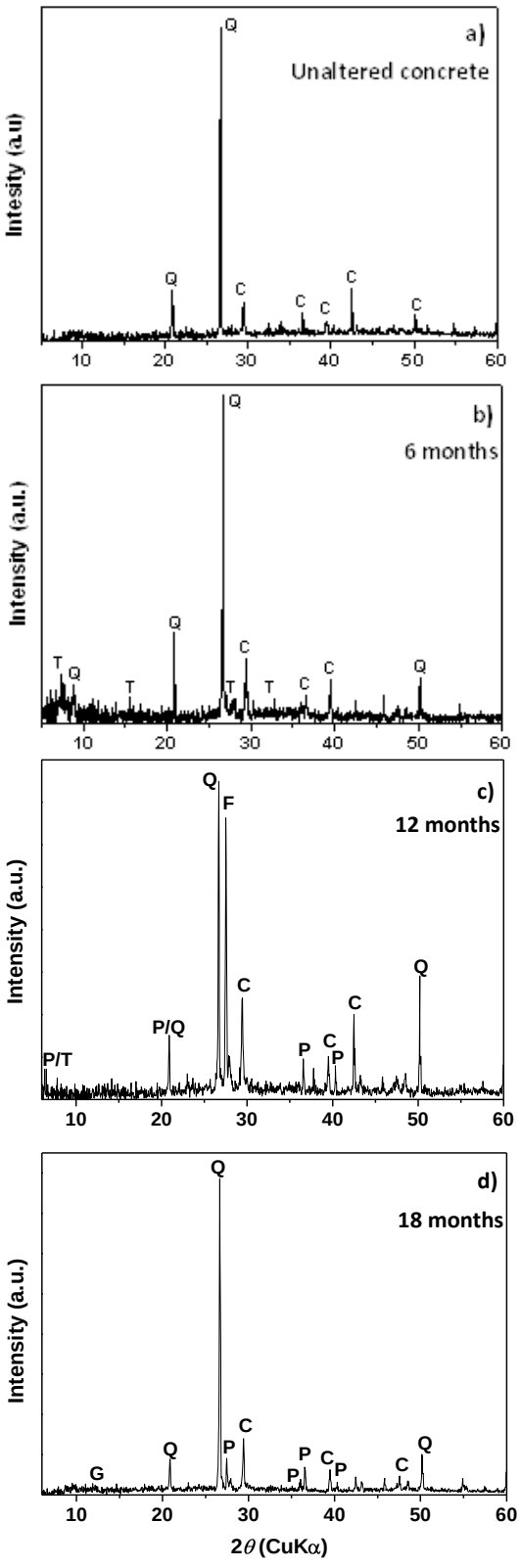

Figure 8. X-ray diffraction pattern of: a) concrete CEM I 42.5R/SR; b) 6 months; c) 12 months; d) 18 months (P = portlandite, T = tobermorite, Q = quartz; C = calcite, B = brucite, F = potassic feldspar, G= gypsum).

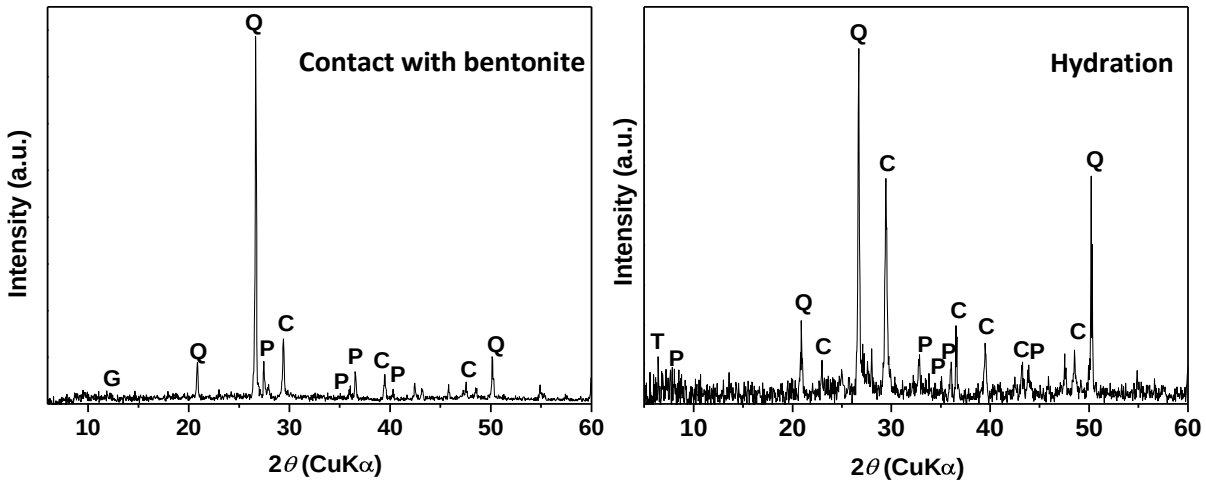

Figure 9. X-ray diffraction pattern of the concrete samples collected from the 18-month tests at the contact with bentonite (bottom part) and at the hydration zone (upper zone of the block) (G = gypsum, B= brucite, Q= quartz, P= portlandite).

2.2.3 FTIR spectroscopy

The structure of C-S-H gel is very complex with a variable Ca/Si ratio corresponding to different molecular structures. FTIR spectroscopy turned out to be very useful in determining the cement chemistry due to the poor crystallinity of silicate hydrates [62]. FTIR spectra recorded for the unaltered CEM I SR and the samples collected from the 6, 12 and 18-month test are shown in Figure 10.

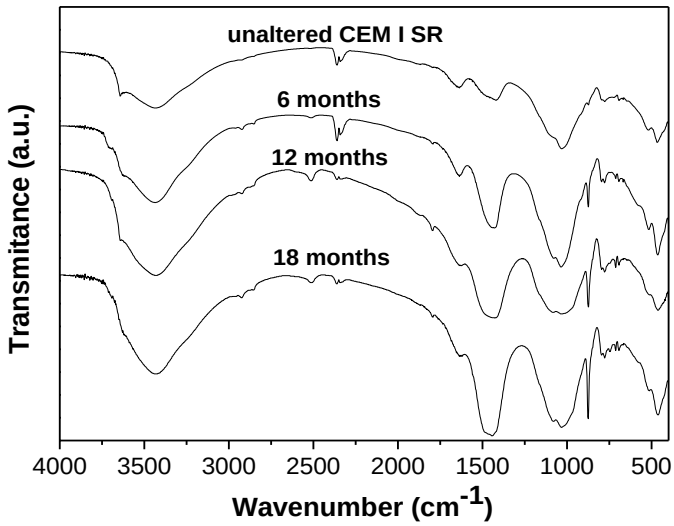

Figure 10. FTIR spectra of: a) unaltered CEM I-SR; b) sample from the 6-month test; c) sample from the 12 month-test; d) sample from the 18-month test.

Table IX summarizes the phases identified in Figure 10 and their corresponding wavenumbers.

Table IX. Phases identified in the FTIR spectra shown in Figure 10.

Phase	Wavenumber (cm^{-1})			
	CEM I SR	**6 months**	**12 months**	**18 months**
Brucite		3700		
Portlandite	3641	3632	3628	3636
Vaterite				1492
Aragonite				1460
Calcite	1425	1440	1440	1434
	876	873	871	875
	709	710	715	715
C-S-H gels	1099	1082	1080	1085
	1032	1033	1021	1038

Evolution of the broad band at ~ 2800 - 3750 cm^{-1} is due to stretching vibrations of O-H groups in H_2O or hydroxyls with a wide range of hydrogen bond strengths. Band at 3640 cm^{-1} is due to Ca-OH vibrations from portlandite. The disappearing of this band when leaching proceeds allows us to follow the dissolution process of this solid phase. The band at 3450 cm^{-1} is attributed to hydrogen bonded OH species (O-H-O-H) adsorbed on the surfaces.

Figure 11 shows the mid-IR spectra for CEM I-SR and the samples collected from the dismantled tests. In this case, the observed features provide useful information about Ca/Si ratio in C-S-H silicate polymerization, and the presence of TO_4 tetrahedra in gel chains (T= Si or Al).

In hydrated Portland cements, the main mid-IR band for C-S-H gels appear at 970 cm^{-1} (Si-O stretching vibrations of Q2 tetrahedra), 660-670 cm^{-1} (Si-O-Si bending vibration, which is influenced by Si-O-Si angle and occupancy of neighbouring sites), and 450-500

cm^{-1} [62]. These mid-IR bands change systematically in frequency and/or intensity with Ca/Si ratio in C-S-H, which is also related with silicate polymerization.

The band at 970 cm^{-1} is attributed to Si-O stretching vibrations in C-S-H gels with jennite type structure. Amorphous aluminosilicate phases are likely to cause vibration at around 1070-1080 cm^{-1}. The appearance of a shoulder at ~1200 cm^{-1} occurs for gels C-A-S-H with structure 1.1 nm tobermorite type (Ca/Si>0.8), because of its occurrence for natural aluminosilicates [63].

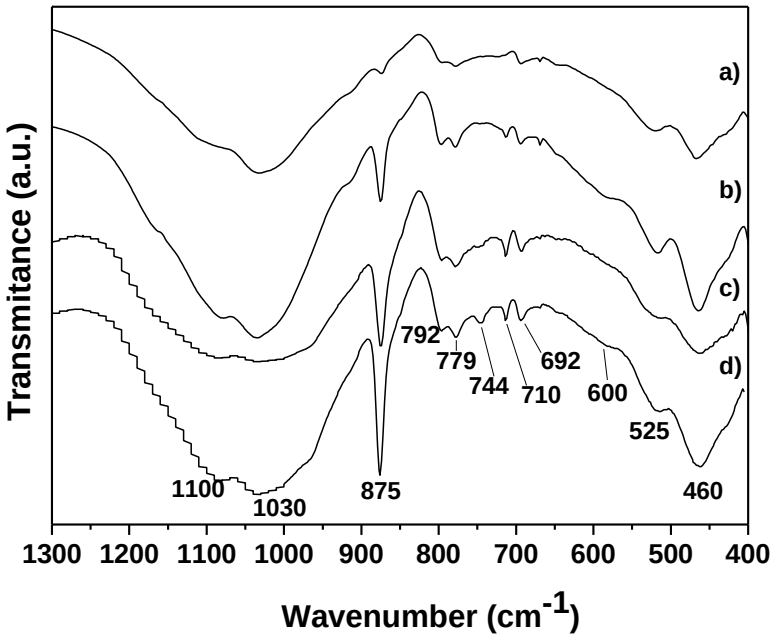

Figure 11. Mid-IR spectra of: a) unaltered CEM I-SR; b) sample from the 6-month test; c) sample from the 12 month-test; d) sample from the 18-month test.

The bands in the range 500-400 cm^{-1} are due to deformation of TO_4 tetrahedra (T= Si or Al), and the increasing in intensity of this bands, when leaching proceeds, is also consistent with and increasing in polymerization (more bridging TO_4 units linking dimmers). Moreover, intensity of the out-of-plane bending Si-O vibration at 525 cm^{-1} decreases, when leaching proceeds, as a result of polymerization of SiO_4^{4-} units in cement.

Characteristic ettringite bands normally appear at 1100 and 610 cm^{-1} (32). However, the Si-O stretching bands can eventually obscure the SO_4^{2-} bands of ettringite. Broad bands centered at ~1110-1130 cm^{-1} can be attributed to C-S-H gels with Ca/Si < 1.4 [62] overlapping ettringite main band.

The characteristic bands of calcite were found in the reference and test samples at 1425-1440 cm^{-1}, ~875 cm^{-1} and ~710 cm^{-1}. In the 18-month test, vaterite and aragonite bands were also distinguished. Carbonation of samples is assumed to occur during the storing of samples. However, the intensity of the 1425 and the 875 cm^{-1} bands was increasing with test time. So, apart from the inevitable carbonation during storage, calcite was formed as a consequence of the leaching in concrete.

2.2.4 SEM microscopy

Unaltered concrete

C-S-H gels were the only phases that could be identified during the SEM observation of unaltered concrete (Figure 12).

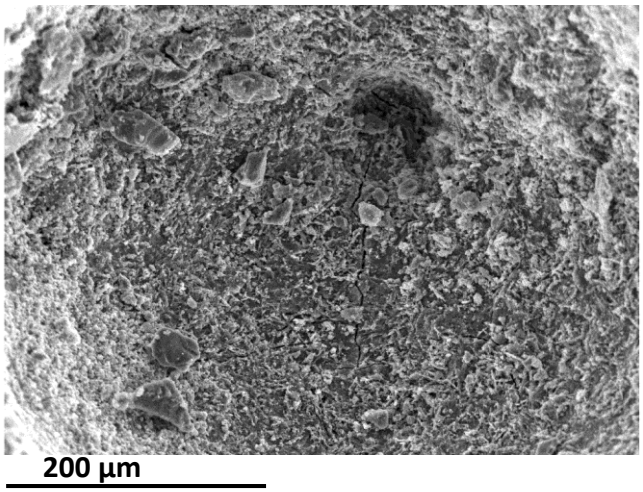

Figure 12. SEM image of C-S-H gels formed in a concrete pore.

Concrete from the 6-month test.

Calcite precipitation occurred at the hydration zone. Carbonation was observed in the three tests, although its extension increased with test time.

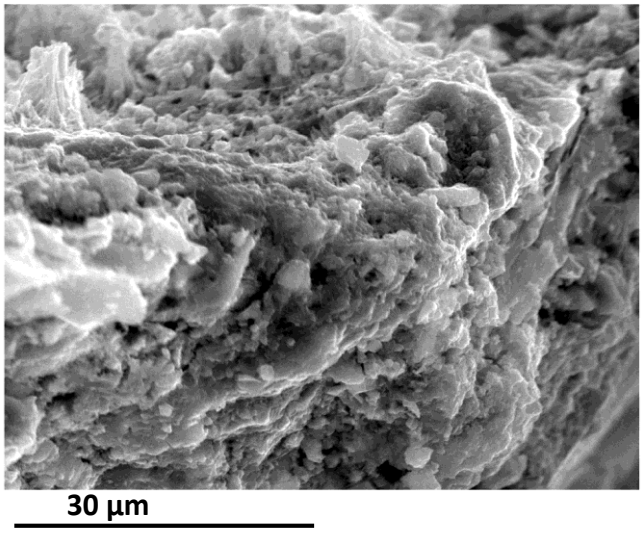

Figure 13. Calcite found in a concrete sample collected at the hydration zone in the 6-month test.

Portlandite [$Ca(OH)_2$] was identified in pores close to the concrete-bentonite interface. Figure 14 shows several portlandite plates found in one of the concrete pores at the interface.

Numerous structures were distinguished during the SEM characterization. These phases exhibited different Ca/Si ratios (Figure 15). Acicular crystals were frequently seen in the concrete pores (Figure 16). Although, this morphology is typical for ettringite, EDS analysis detect negligible amounts of sulphur. Some zeolites and calcium magnesium silicates hydrates exhibit such crystal habit.

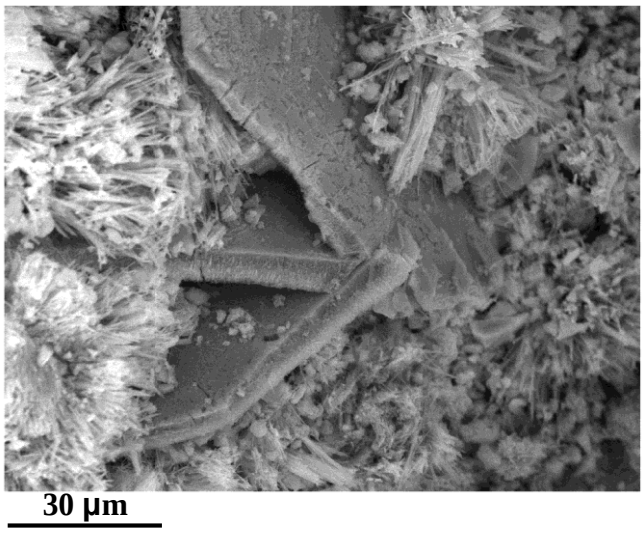

Figure 14. Portlandite plates found in a concrete pore near the concrete/bentonite interface.

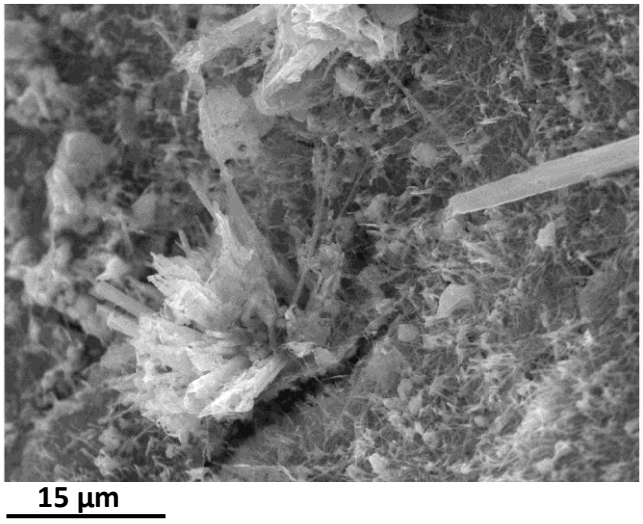

Figure 15. Unidentified C-S-H phases found in one of the concrete pores together with portlandite.

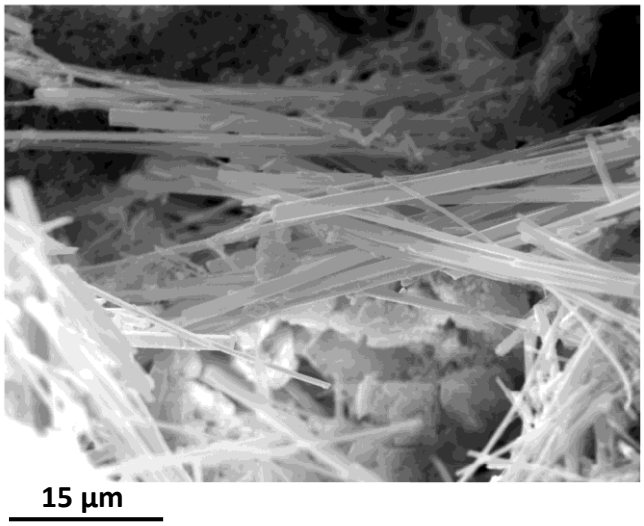

Figure 16. Acicular precipitates found in the concrete pores in the 6-month test.

In areas close to the concrete/bentonite interface, dissolution marks appeared on the surface of the aggregates. Clay minerals and quartz dissolution can enhance the precipitation of C-S-H gels.

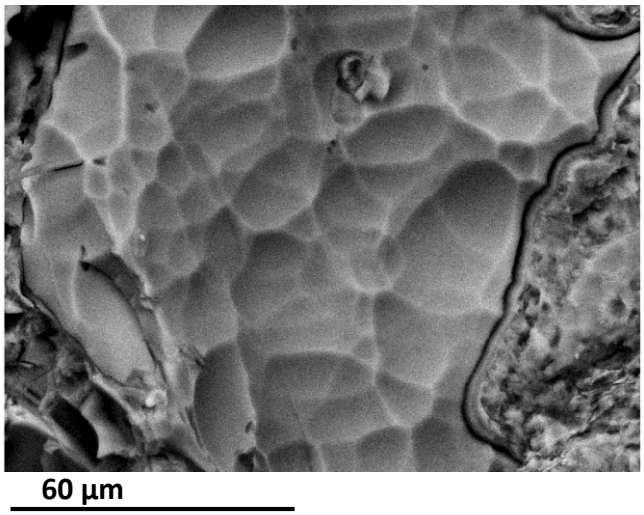

Figure 17. Dissolution marks in concrete aggregates.

Concrete from the 12-month test.

In the 12-month test, calcite formation was observed at both, the hydration zone and inside the concrete pores (Figure 18).

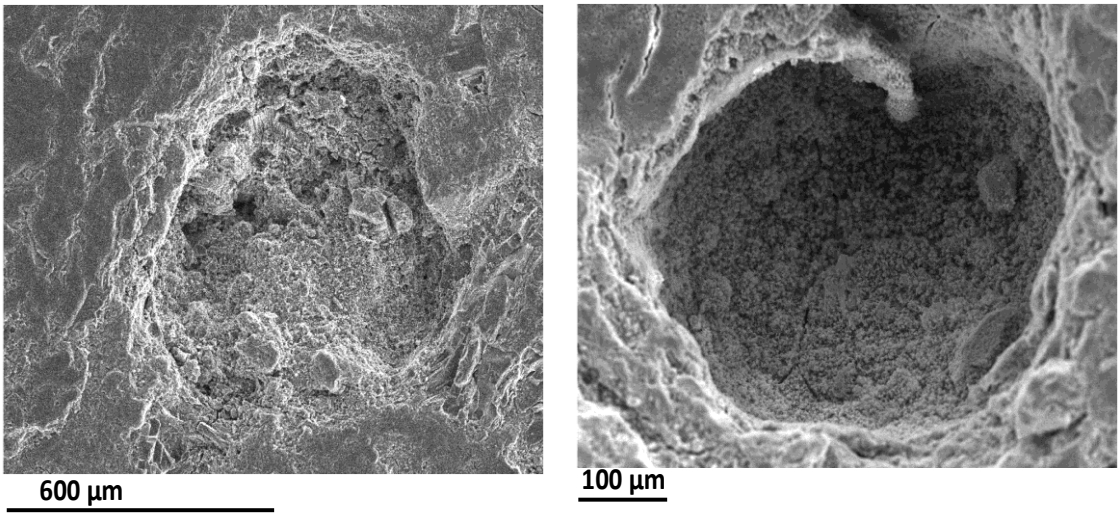

Figure 18. Surface of a pore formed in the concrete block in the 12-month test.

Figure 19 shows different SEM images corresponding to different calcite morphologies found in several pores formed along the bentonite block. Calcite was found in the contact with hydration, as in the 6-month test. After 12 months, calcite started to precipitate in the concrete pores close to the bentonite contact.

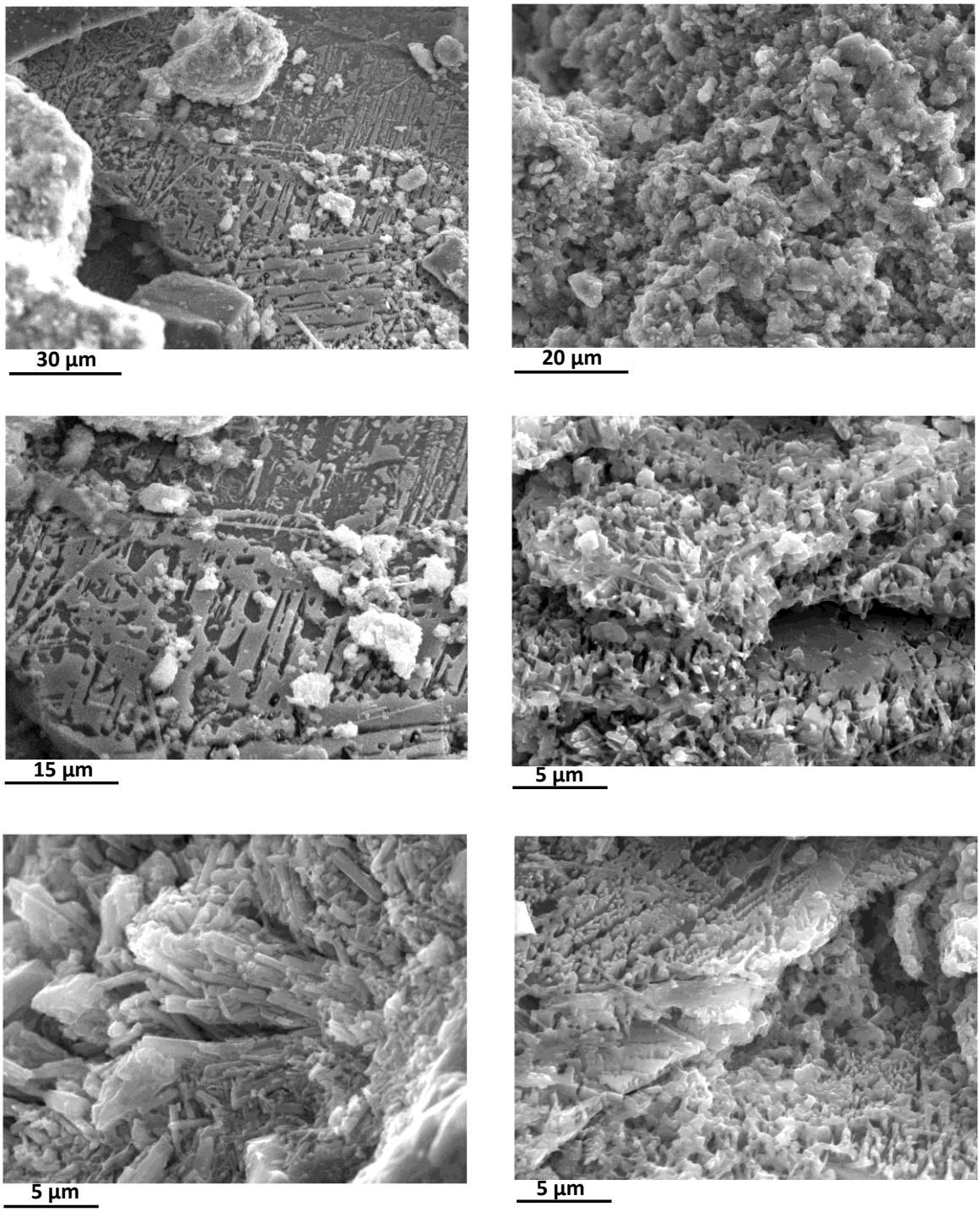

Figure 19. Calcite crystals observed in the concrete pores in the 12-month test.

Apart from calcite and CSH gels (Figure 20), ettringite crystals were also observed inside the concrete pores closer to the concrete/bentonite interface (Figure 21). Ettringite is a hydrous calcium aluminium sulfate mineral with formula $Ca_6Al_2(SO_4)_3(OH)_{12}\cdot 26H_2O$. The combined effect of the heating (water content and

temperature variations) and an external source of sulfates (hydrating solution) favors its formation.

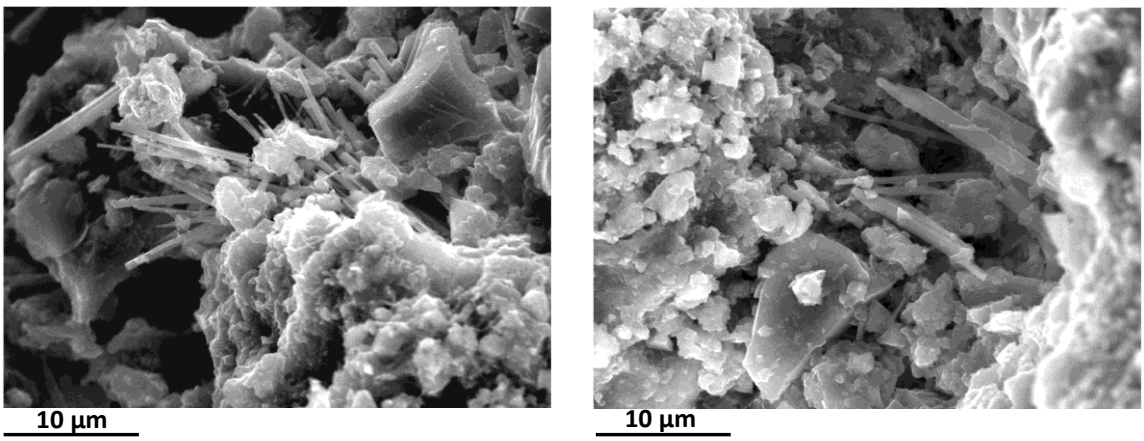

Figure 20. C-S-H gels found inside two different concrete pores.

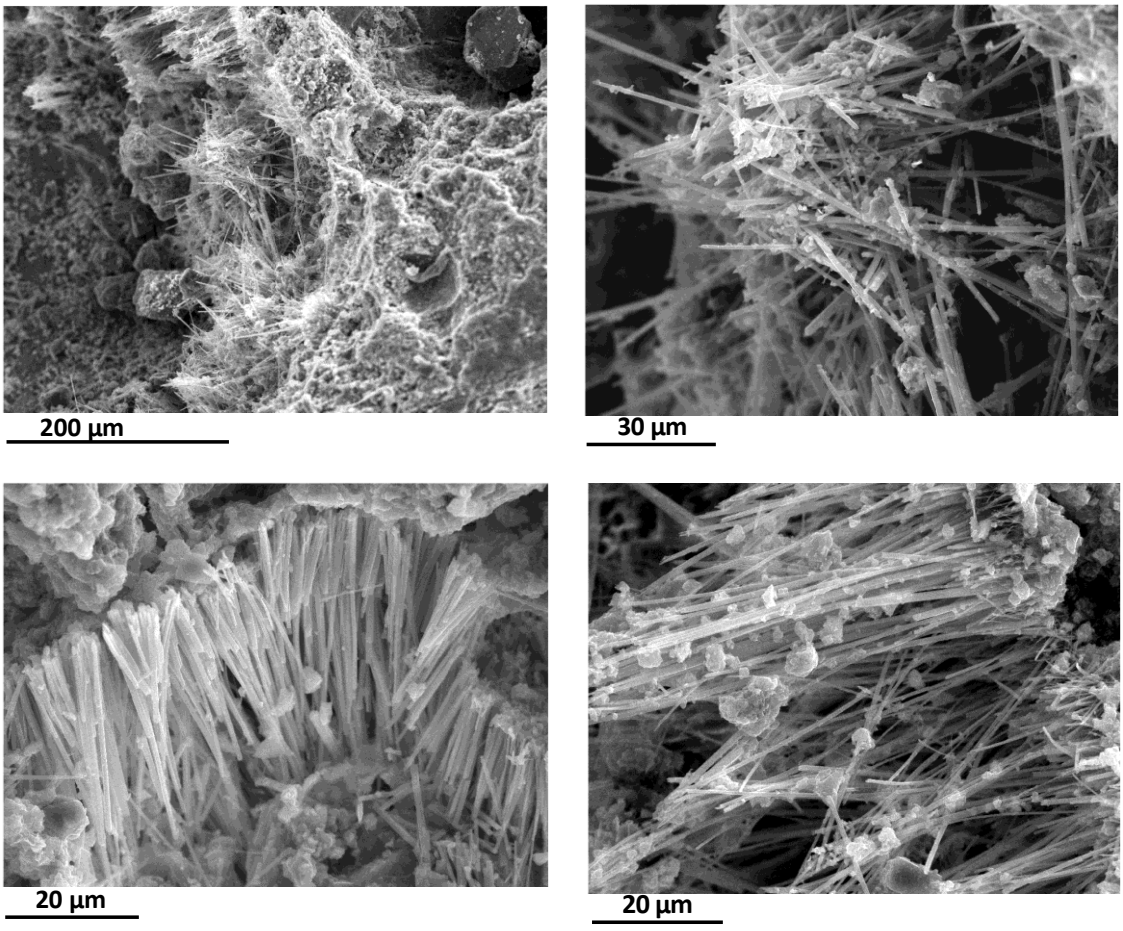

Figure 21. Ettringite crystals found in the concrete block from the 12-month test.

Concrete from the 18-month test.

SEM characterization of the concrete block from the 18-month test confirmed the formation of Ca-rich phases (Figure 22), C-S-H gels (Figure 23) or ettringite (Figure 24), previously seen in the 6 and 12-month tests.

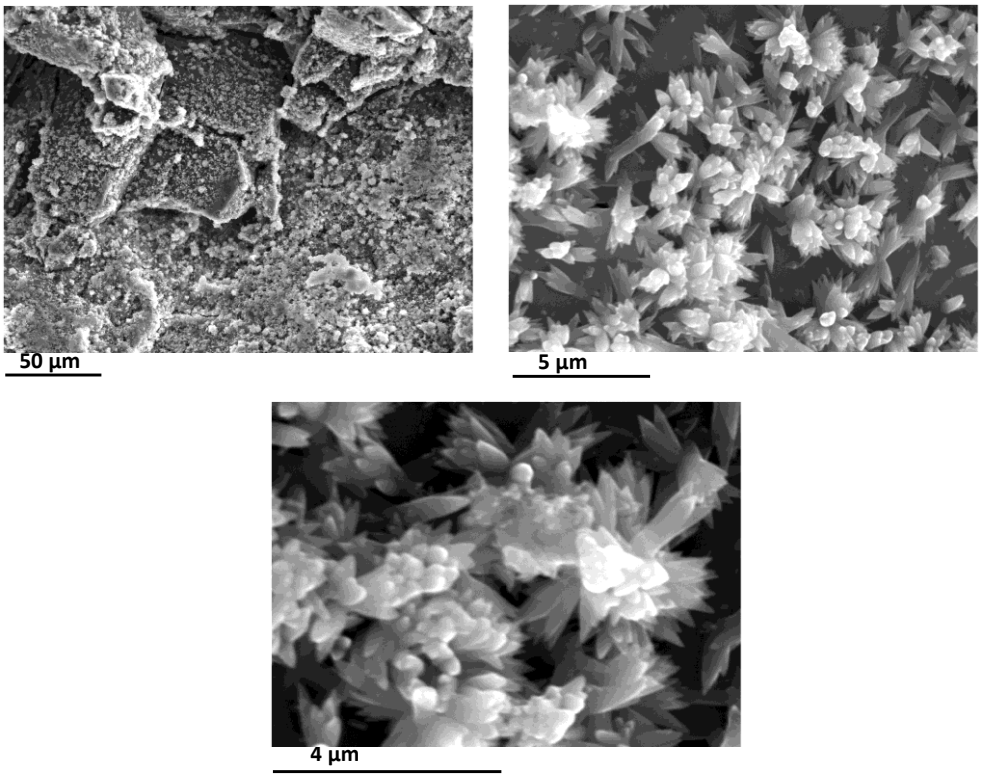

Figure 22. Calcium-rich phases precipitation in the concrete block from the 18-month test.

Calcium phases precipitation seems to increase at longer test times. For their morphologies it cannot be unambiguously determined as carbonates or portlandite. In the 18-month test, portlandite was observed along the whole concrete block, and not just near the concrete/bentonite interface.

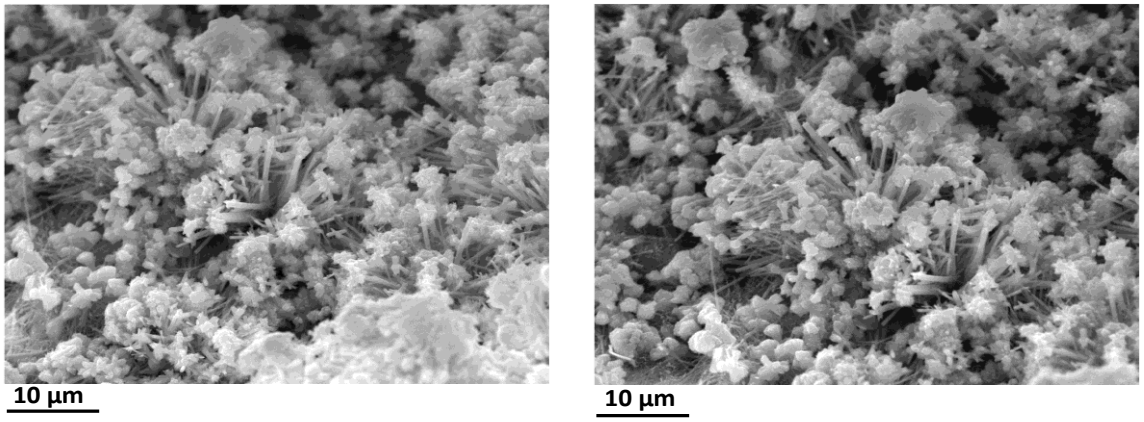

Figure 23. C-S-H gels found inside the concrete pores in the 18-month test.

Near the concrete/bentonite interface, gypsum (or thaumasite) was detected in some of the concrete pores. EDS confirmed the presence of sulfate, but in this case, sulfur content (%at.) was higher than in ettringite crystals.

Due to the high content of sulfate in the hydrating solution, formation of sulfate-rich phases, such as gypsum or ettringite, was expected.

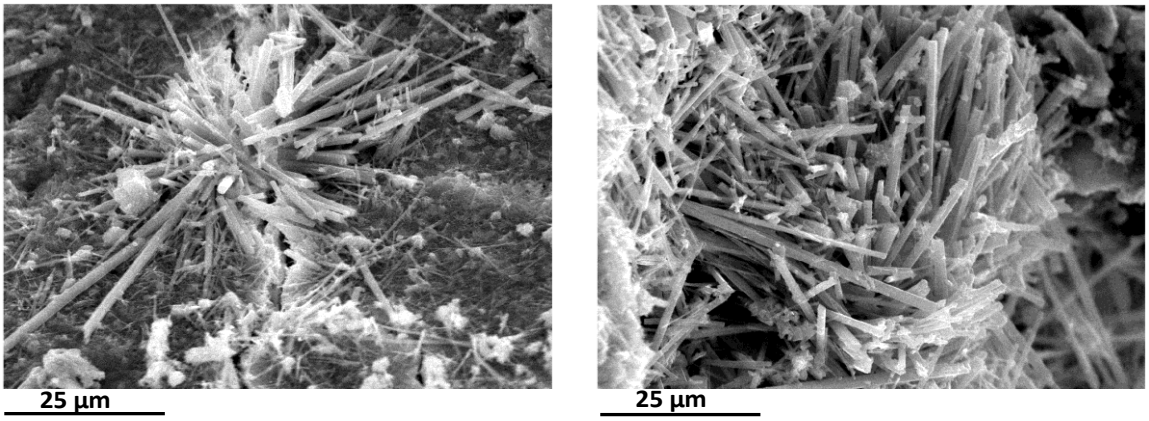

Figure 24. Sulfate -rich phases grown inside a concrete pore in the 18-month test.

EDS mapping was conducted on concrete from the dismantled tests in areas close to the concrete/bentonite interface. EDS maps corresponding to Ca, Si and S are shown in Figure 25. Decalcification could not be confirmed. However, a significant increase in the sulphur content was observed as test time increased.

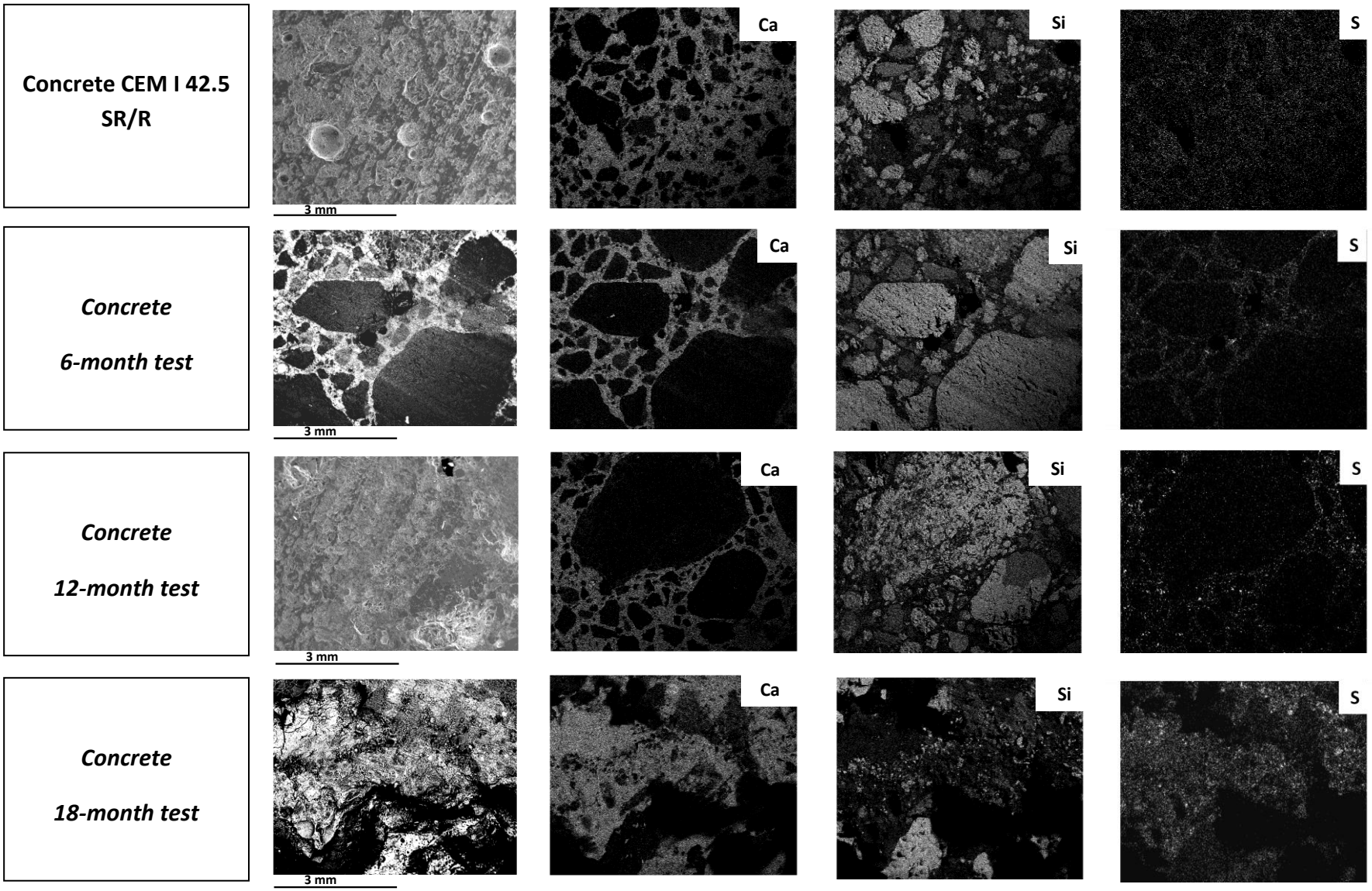

Figure 25. EDS mapping of Ca, Si and S of CEM I 42.5 SR/R (a) and concrete in contact with bentonite for 6 months (b), 12 months (c) and 18 months (d).

2.3 Discussion

2.3.1 Sulfate attack

Results presented in this section indicate that sulfate attack of the Portland concrete blocks is a progressive phenomenon from the hydration surface inwards and involves several stages. These data agree closely with the mechanism of sulfate attack proposed by Gollop and Taylor [64].

Based on the results reported in literature and presented in this work, the sequence of attack is schematically illustrated in Figure 26 and it has the following stages:

1) Diffusion of SO_4^{2-} and CH (Calcium Hydrate) leaching.
2) Ettringite formation
3) Gypsum formation and depletion of CH
4) Decalcification of C-S-H
5) Thaumasite formation.

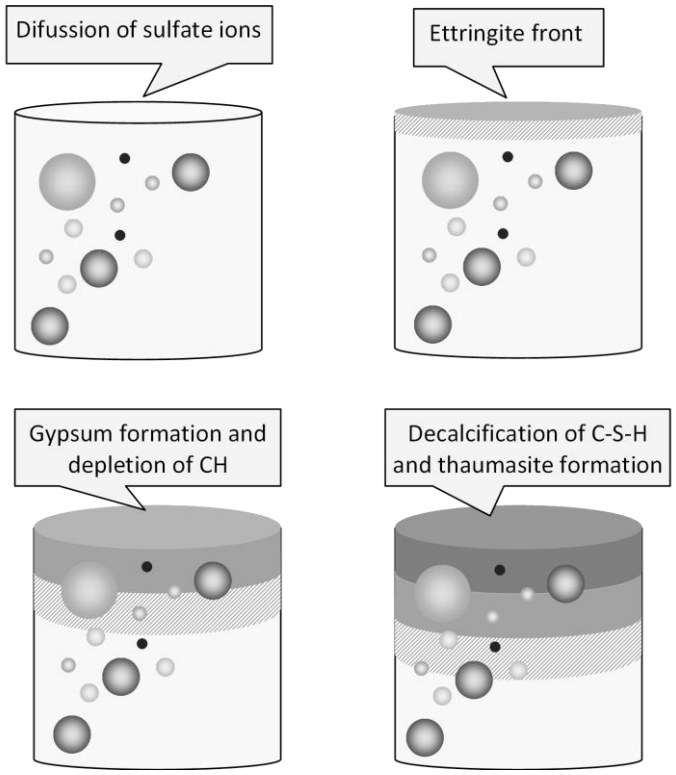

Figure 26. Schematic representation of the sequence of sulfate attack in portlandite cement.

a) Diffusion of SO_4^{2-} and CH (Calcium Hydrate) leaching

According to literature, at early stages of the sulfate attack, sulfate diffusion process occurs complementarily to CH leaching. The intensity of this ion flow depends on the porosity of the block, the changes in porosity caused by the sulfate attack and the concentration gradient. An increase of Ca^{2+} concentration was also observed at this step [65].

b) Ettringite formation

Ettringite is formed by the reaction of SO_4^{2-} with the AFm phase (i.e. monosulfoaluminate and monocarboaluminate). According to Gallop and Taylor (30), ettringite detected by XRD is a well-crystallized compound that forms in cracks or voids. Ettringite can also be formed as a result of reaction between SO_4^{2-} and the ferroaluminate phase [64, 66].

Ettringite was observed mainly in void pores, but it could not be detected within the paste or transition zones. Ettringite is the first attack product detected in the surface at early ages and it is the vanguard of the attack front.

c) Gypsum formation

When the alumina supplied by the AFm phase is deficient, ettringite precipitation ceases and the SO_4^{2-} react with Ca^{2+} initiating the gypsum crystallization [67]. Consequently, this reaction consumes Ca^{2+} from solution and more CH is decomposed into the pores causing CH depletion.

In literature [68], gypsum tends to precipitate beyond the maximum distribution of ettringite.

As gypsum results from a CH substitution reaction, the amount of CH and its localization play a decisive role. At early hydration stages, precipitation of CH causes massive deposits of crystals on the paste-aggregate interface, which leads to the inevitable increase of porosity in this region.

In the corroded concrete surfaces, the complete depletion of CH caused by gypsum formation is also accompanied with a deposition of calcium carbonate (calcite) crystals, which could cause a decrease in the amount of gypsum due to the decomposition of solid phases containing sulfate. For this degradation stage, concrete shows a dominant gypsum environment and the C-S-H will be affected reducing its intrinsic strength and stiffness [67, 69].

d) C-S-H decalcification

Decalcification of C-S-H could be expected causing modifications in the chemical and microstructural composition of concrete [70]. Decalcification of C-S-H depends on the

depth. The area closer to the hydration surface would have a higher degree of decalcification.

e) Thaumasite formation

According to Collepardi (45), thaumasite may form from reaction of calcium carbonate, calcium sulfate, the C-S-H, and water. Some authors propose that ettringite exerts a catalytic effect on thaumasite formation [71].

The main differences between ettringite and thaumasite formation reported by Collepardi [71] are:

I. Ettringite causes expansion, but even after cracking the material still remains sound and cohesive. Conversely, thaumasite causes the mortar to become incoherent and non-resistant.

II. The presence of thaumasite is often preceded by the formation of ettringite. Ettringite is always found in the early stages of the sulfate attack. In the attack front, profile compounds also confirm that the deeper attack front is characterized by ettringite formation. The final stage is characterized by the presence of thaumasite in the outer surfaces.

Deterioration of concrete caused by ettringite and thaumasite occurs in several forms including:

- Expansion
- Cracking
- Spalling
- Loss of strength
- Adhesion

Ettringite formation is, in general, associated primarily with expansion, cracking and spalling. On the other hand, thaumasite formation is accompanied by a more severe damaging effect, which is able to transform hardened concretes or mortars in a pulpy mass because of the loss of strength.

According to Mehta [67], the physical mechanism by which ettringite causes expansion and cracking is based on swelling of ettringite by water adsorption and on topochemical formation of ettringite with directional crystal growth. However, these mechanisms alone cannot explain the loss of strength and adhesion, which always accompanies sulfate attack. Mehta thinks that some strength loss occurs before ettringite forms and swells due to water adsorption. When sulfate sources other than calcium sulfate are available, i.e. sodium, potassium or magnesium salts, gypsum forms

by consuming Ca^{2+} from both $Ca(OH)_2$ and C-S-H. Therefore, gypsum formation would be accompanied by decomposition of $Ca(OH)_2$ and C-S-H. Since C-S-H is the primary source of strength, the reduction in C-S-H, rather than gypsum formation itself, would be responsible for the strength loss accompanying the sulfate attack. However, this strength loss mechanism, based on gypsum formation and C-S-H decomposition, cannot work when ettringite forms and calcium sulfate is the salt initially available for sulfate attack. In other words, when ettringite forms without preliminary gypsum formation, no strength loss should occur since C-S-H is not consumed.

On the other hand, thaumasite formation consumes C-S-H independently of the type of sulfate salt. Because of the formation of C-S-H and $CaCO_3$ to thaumasite, a significant strength loss was registered and the specimen was completely destroyed. Since C-S-H has been consumed in thaumasite formation, this process produces significant strength loss, even in the absence of a preliminary gypsum formation process.

2.3.2 C-S-H gels

Poorly-crystalline calcium silicate hydrates (C-S-H gel) are the primary hydration products of Portland cements, and may constitute up to 70% of hardened cement pastes. Thus, the properties of these gels are important for the mechanical and chemical properties of cement based materials. C-S-H gels are commonly formed via the hydration of C_3S and β-C_2S, which are the principal constituents of Portland cement clinker. In hardened cement pastes, C-S-H gels are nanoheterogeneous, showing variable composition on a micrometric scale [38, 72]. The C-S-H phases are often defined by their molar CaO/SiO_2 (C/S ratio). For C-S-H gel in fully reacted hydrated cement pastes it may vary over the range 1.7-2.0 (most probably 1.7-1.8) [38].

Ageing, carbonation, leaching, alkali-silica reaction (ASR), etc. meanwhile may cause the C/S ratio to drop well under 1.0.

In order to understand the structure of C-S-H phases and the processes of their formation, many investigations have been carried out of both, hardened cement paste and synthetically produced C-S-H gels.

Because of the possibility of intimate mixing of C-S-H gel with portlandite, some authors have suggested an actual upper limit of the C/S ratio of about 1.5 [49], whilst several authors investigated C-S-H phases for a possible miscibility gap, which may be present at around C/S=1.0 [4].

The most frequent C-S-H phases and their corresponding C/S ratio are shown in Table X.

Table X. C-S-H phases and their corresponding C/S ratio.

C-S-H gels: Ca/Si ratio	
Phases	**Ca/Si ratio**
Truscottite	0.583
Gyrolite	0.66
Tobermorite	0.83
Xonotlite	1
Scawtite	1.16
Foshagite	1.33
Jennite	1.5
Hillebrandite	2
Afwillite	9

C-S-H phases are usually masked by calcite and portlandite, so their identification is difficult. C/S ratios obtained by dot EDS analysis are usually not accurate. During this work, an attempt for identifying the C-S-H phases was made. Elemental atomic relations were calculated on the basis of dot analysis. In Table XI, the C/S ratio calculated for several dot analysis and the possible C-S-H phases are shown.

Table XI. C/S ratio calculated for the spot EDS analysis carried out in 6-month and 18-month concrete samples and the corresponding C-S-H phases.

Cell 1 (6-month test)		**Cell 2 (12-month test)**		**Cell 3 (18-month test)**	
C/S ratio	**Phase**	**C/S ratio**	**Phase**	**C/S ratio**	**Phase**
0.63	**Tobermorite**	0.6	**Tobermorite**	0.65	**Tobermorite**
1.36	**Foshagite**			0.96	**Xonotlite**
1.80	**Jennite**			1.77	**Jennite**
3.08	**Afwillite**			2.03	**Hillebrandite**

Jennite was identified by FTIR analysis in the 3 cells dismantled, not only by EDS analysis. Tobermorite was found in the X-ray diffraction pattern recorded for concrete samples collected from the 6, 12 and 18-month test.

2.4 Conclusions

In the three cells dismantled, sulfate-rich phases, such as gypsum and ettringite, were identified by means of FTIR, XRD and SEM analysis, basically inside the pores near the concrete/bentonite interface.

Porosity increased with time due to the dissolution of the concrete matrix.

High concentration of sulfate in the hydrating solution, together with the leaching of salts from the upper areas is responsible for the formation of these new phases close to the interface.

Decalcification of the concrete surface in contact with hydration occurred, as well as carbonation.

3. Concrete/bentonite interface

3.1 Introduction

Concrete degradation generates a diffusive alkaline plume, which can affect the swelling and transport properties of the bentonite, as well as the properties of the adjacent host rock and groundwater. Many studies have been performed in order to study the influence of alkaline media on bentonite. Eberl *et al*. [3] reported that the formation of illite or illite/smectite depends on the solution concentration rather than on temperature and time of reaction [4, 5]. Formation of mixed layer phases seems to be an intermediate step in a series of dissolution-precipitation processes, including the formation of zeolite minerals.

Cuevas *et al*. [6] carried out a set of batch (alkaline solution and bentonite (25-200 ^{o}C) and column experiments (granitic and alkaline water-mortar-bentonite, 25-120 ^{o}C) in order to study the influence of alkaline media on FEBEX bentonite. The main phases identified in the alkaline reaction of FEBEX bentonite are phillipsite, Mg-clays, analcime, tobermorite and C-S-H gels. The formation of a new smectitic tri-octahedral phase was confirmed, as well.

During the ECOCLAY project [7], three different series of tests were performed:

a) Batch leaching test, where bentonite was mixed with four synthetic cement porewater solutions.

b) Cell tests using MX-80 bentonite compacted to a dry density of 1.4 and 1.6 g/cm^3 with subsequent drilling of a hole in the bentonite and filling it with fresh cemen paste. This closed system was examined after 3 to 12 months with respect to chemical and microstructural changes.

c) In the third tests series, a hardened cement disc was placed in contact with bentonite and the system was percolated by granitic water. The quantity of dissolved smectite was found to depend on the water content. The average amount of dissolved smectite was found to be 12 g of smectite per litre of pore solution, i.e. 1.2% under the prevailing closed conditions.

Theoretical considerations [8, 9] and experimental data have indicated that zeolites like phillipsite and analcime are by-products of the alkaline reaction. Mg^{2+} uptake and selectively enrichment in the montmorillonite crystal lattice, when the Aluminum octahedral clusters are being dissolved yielded saponite.

The most important conclusions from these earlier studies were:

- High alkali cement degrades quicker than low alkali cement. The latter deteriorates by destruction of the C-A-H gel.

- Dissolved elements and water migrate from the fresh cement paste to the bentonite in the first few hours.
- The cement paste is dehydrated and its voids become wider; water moves from the bentonite to the dense cement matrix.
- The dense paste fissures.
- pH=12.6 seems to be the threshold value for significant changes of the smectite component at the experimental times of the test performed.
- Ca migrates from the cement to the clay causing ion exchange and change in the microstructure of the clay by coagulating softer parts.

Models show that solution composition is first controlled by the release of NaOH and KOH, leading to very high solution pH (>13). In a second step, the solution composition is controlled by portlandite ($Ca(OH)_2$ – pH 12), and finally by calcium-silicate-hydrate (C-S-H) phases (pH 9-10).

As a consequence, numerous investigations have been conducted on the stability of clays under such high pH conditions [3-5, 17-25]. These studies consistently indicate that the clay minerals described in the Callovo-Oxfordian formation of the MHM site (smectite, illite and mixed-layer illite-smectite [26, 27]) would react when in contact with high-pH alkali-rich solutions. For example, high-pH experimental investigations on smectite-type minerals indicated a fast montmorillonite-to-beideillite transformation [28].

The scope of the present section is to provide experimental data about the alteration products at the concrete/bentonite interface and the related changes of the bentonite properties in contact with the concrete.

3.2 Results

3.2.1 SEM characterization

Leaching of the most soluble elements, such as alkalis from hydroxides or calcium from portlandite ($Ca(OH)_2$), leads to the increase of pH and the precipitation of phases like brucite and Calcium-rich phases on the bottom part of the concrete blocks (Figure 27.

A continuous layer of Mg and Ca-rich phases was found in the three cells dismantled (Figure 28). This layer was grown on the surface of the bentonite block. According to the EDS profile, in the 18-month test the layer is 2-µm thick (Figure 28).

The Ca-rich layers observed by means of SEM were quite homogeneous. They can be carbonates or portlandite that precipitated on the bentonite surface, and can have a strong impact on the decrease of permeability in compacted bentonite. These phases can have a clogging effect on the bentonite pores.

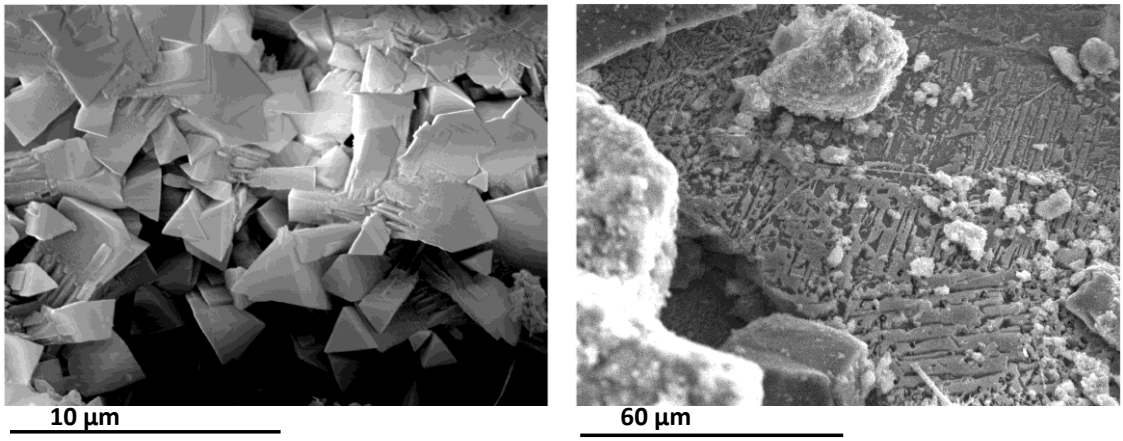

Figure 27. Brucite (left) and calcite (right) precipitated on the bottom surface of the concrete block in the 18-month test.

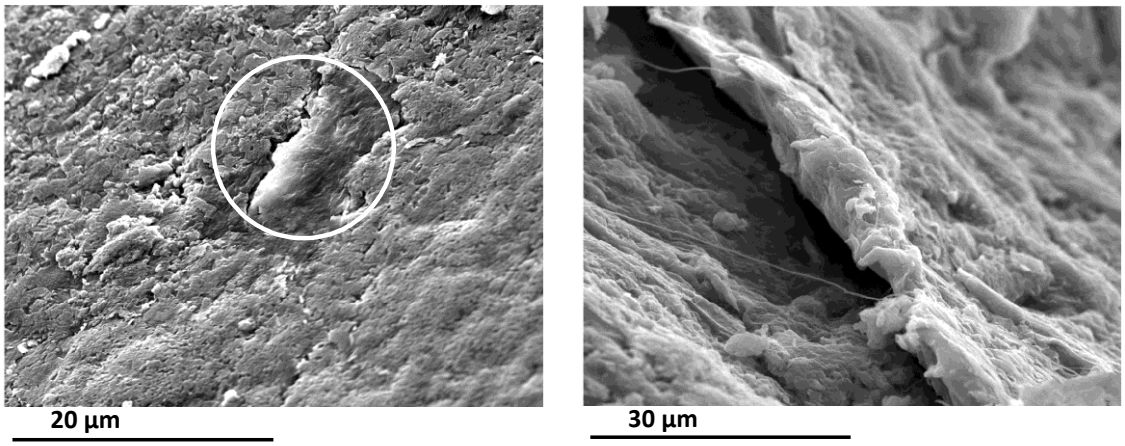

Figure 28. Ca-rich matrix layer grown on the surface of the bentonite block in the 18-month test.

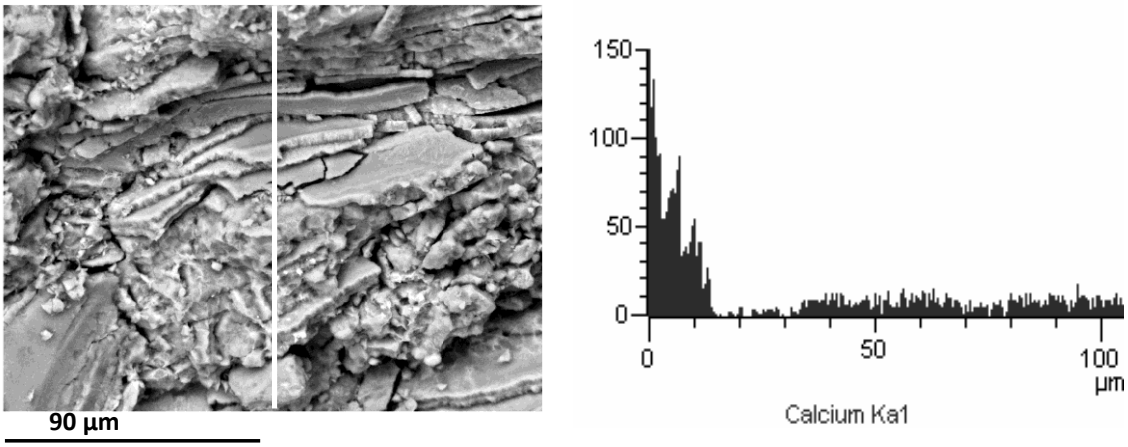

Figure 29. Transversal cut of the Ca-rich gel (portlandite ?) layer in the 18-month test and its corresponding EDS analysis.

C-S-H gels were found below the portlandite layers. Tobermorite-type phases (Ca/Si molar ratio of 0.6) were identified together with brucite and ettringite (Figure 30). In the 18-month test, marks of dissolution of quartz were observed. This process enables the precipitation of C-S-H minerals, such as tobermorite.

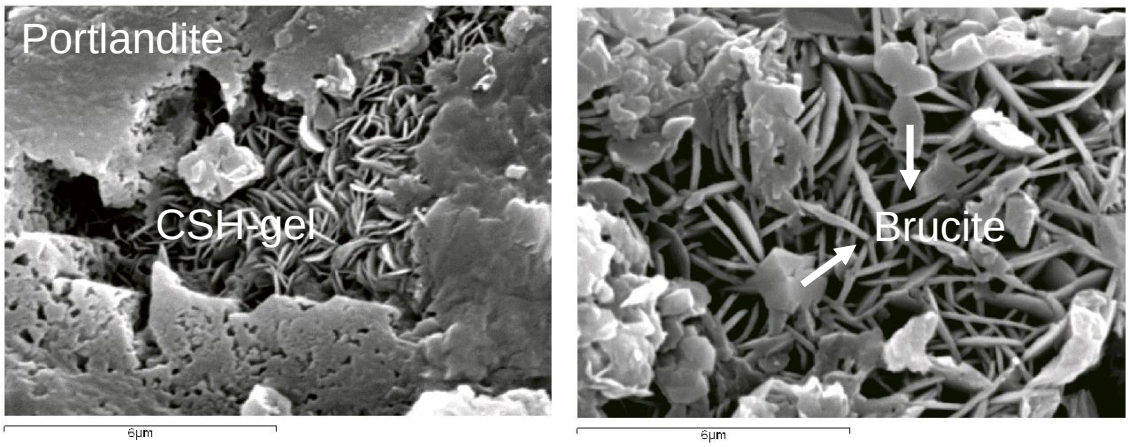

Figure 30. Newly-formed phases at the concrete/bentonite interface at the 12-month test.

Ettringite was precipitated at the upper surface of the bentonite block, both in the 12 and 18-month tests. The formation of sulfate-rich phases is a consequence of the sulfate-rich leachates.

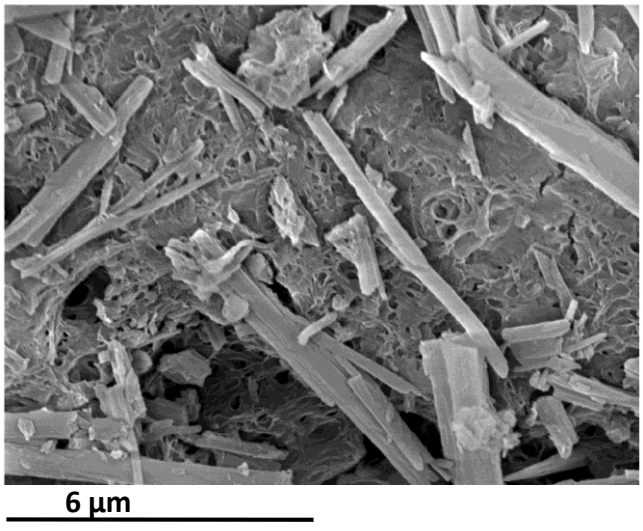

Figure 31. Ettringite found at the concrete/bentonite interface in the 18-month test.

3.2.2 FTIR analysis

Bentonite close to the concrete surface and the precipitate found at the interface from the cell dismantled at 18 months were also analysed by FTIR.

These spectra show the main features of clay minerals. A small band that could correspond to the Mg_3OH deformation of a smectitic trioctahedral phase (saponite-stevensite-talk-like structures) was observed at 669 cm^{-1}. In the spectra of the precipitate three bands at 1417, 874, 712 cm^{-1} reveal the occurrence of calcite. At 3700 cm^{-1}, the spectrum of brucite shows an absorption band. This agrees with the presence of $Mg(OH)_2$ in the precipitate.

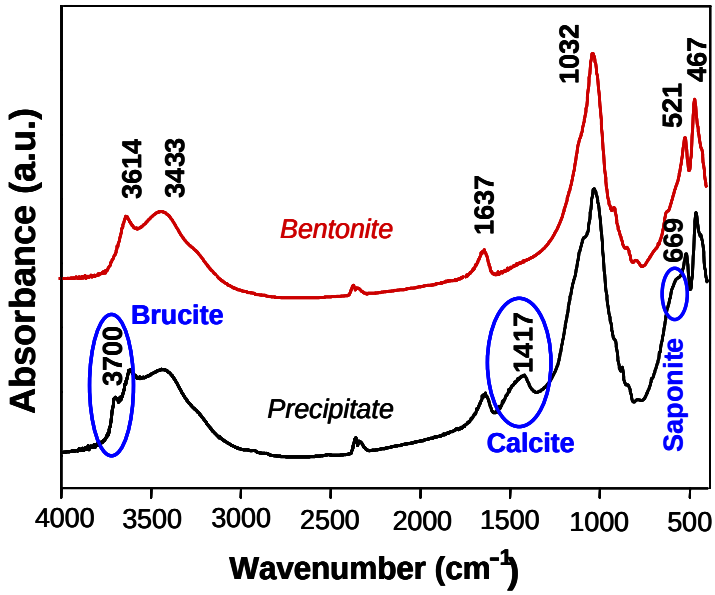

Figure 32. FTIR spectra of FEBEX bentonite and the precipitate found at the concrete/bentonite interface in the 18-month test.

In Table XII, the wavenumbers of the peaks obtained and their assignments (p) denotes peaks found only in the sample containing the precipitate.

Table XII. Wavenumbers of the most intense bands found in the FTIR spectra recorded for the precipitate found at the FEBEX/concrete interface.

Wavenumber (cm^{-1})	**Band assignment**	**Mineral phase**
3700 (p)	OH stretching of structural hydroxyl groups	**Brucite**
3614	OH stretching of structural hydroxyl groups	Bentonite
3433	OH stretching of water	Bentonite
1637	OH deformation of water	Bentonite
1417 (p)	Stretching of calcite	**Calcite**
1032	Si-O stretching	Bentonite
912	Al-Al-OH deformation	Bentonite
874 (p)	Out of plane bending	**Calcite**
839	Al-Mg-OH deformation	Bentonite
712 (p)	CO_3 Out of plane bending	**Calcite**
796	Si-O vibrations of quartz	Bentonite
669	Mg_3OH	**Mg-trioctahedral clays**
521	Al-O-Si deformation	Bentonite
467	Si-O-Si deformation	Bentonite

3.2.3 X-ray diffraction

The presence of brucite in the precipitate found at the interface was assessed by X-ray powder diffraction. A detailed X-ray diffraction study of the bentonite collected at different depths from the interface shows the possible formation of a new phase in the 18-month test. XRD confirmed the formation of a smectitic tri-octahedral phase, as far as neither 1:1 serpentite minerals or talc has been identified. X-ray diffraction pattern shows a peak at 1.53 Å only for bentonite collected from the interface (Figure 33). This reflection line corresponds to a smectitic tri-octahedral phase (saponite-stevensite). XRD analysis of the reoriented aggregates of the fraction below 2 µm shows evidence of the presence of several types of expanding smectite-like phases, because of anomalous increase of the d-spacing and double peak effects. These effects could result from the formation of a brucite-saponite-smectite mixed phase. Brucite-montmorillonite complexes have been characterized and described in bentonite alkaline alteration by Fernandez et al. (2013) [31]. This process does not depend on time, as it can be observed in Figure 34.

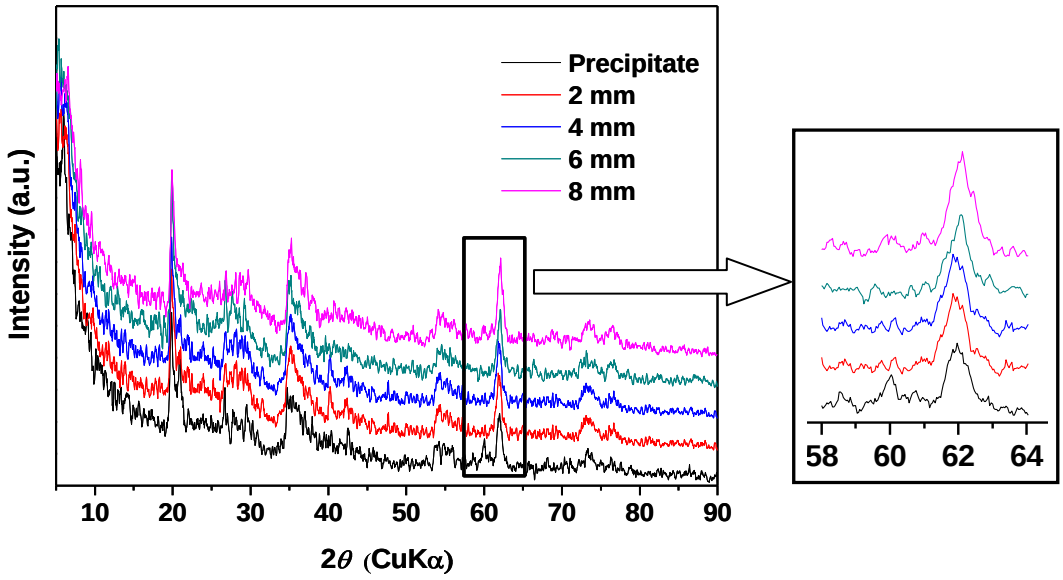

Figure 33. XRD diffraction pattern of bentonite collected at the concrete/bentonite interface in the 12-month test.

Figure 35 shows the XRD patterns recorded for samples collected close to the concrete/bentonite in the 18-month test. Deconvolution of the 57 to 64˚ region corresponding to Figure 35 shows the overlapping of two different bands:

- One centred at 60˚, that would fit the (006) diffraction peak of saponite.

- Another one centred at 62˚, that would correspond to the (006) bentonite diffraction peak.

Negligible differences were observed between the 12 and 18-month test. Both tests seem to confirm the formation of saponite-like phase.

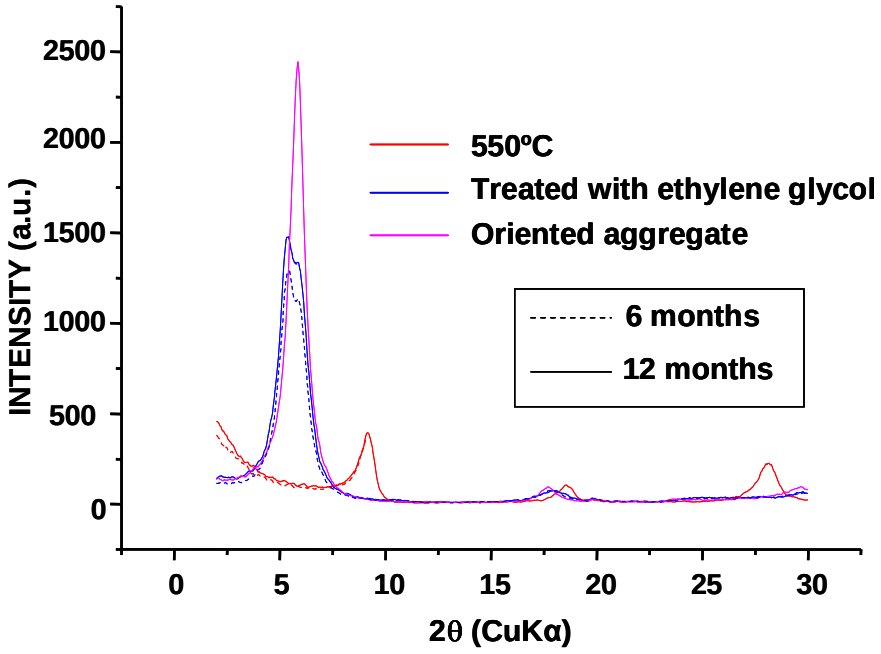

Figure 34. XRD analysis of the reoriented aggregates of the fraction below 2 µm from the bentonite samples collected at the interface in the 6 and 12-month tests.

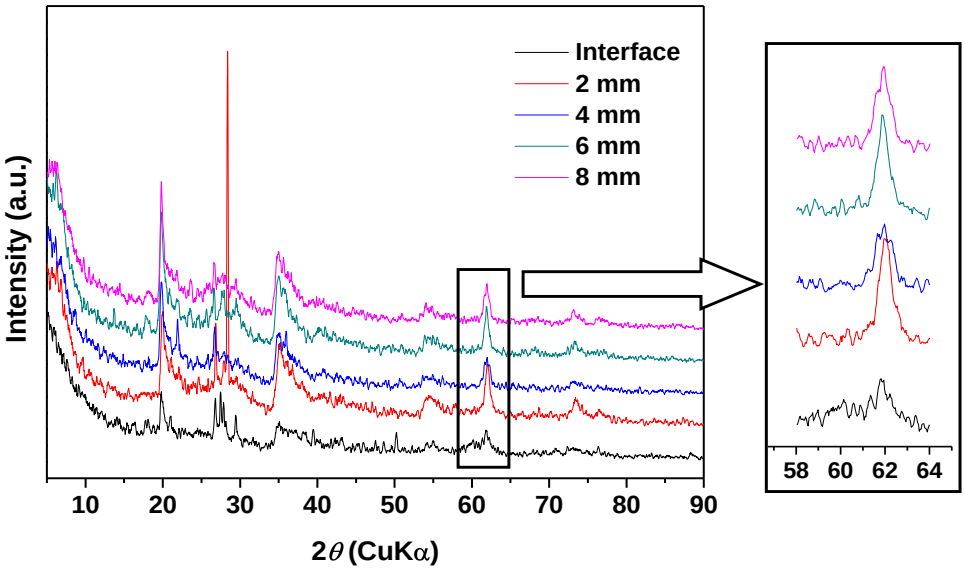

Figure 35. X-ray diffraction pattern of bentonite collected at the concrete/bentonite interface in the 18-month test.

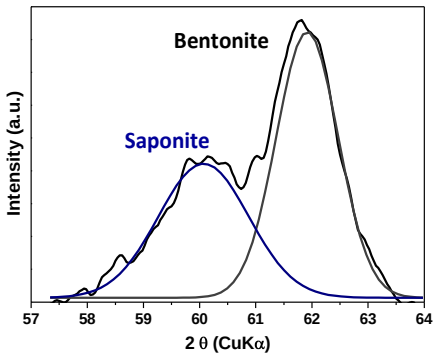

Figure 36. Deconvolution of the 57 to 64˚ region in the previous XRD pattern.

3.3 Conclusions

Characterization of the concrete/bentonite interface confirmed that the alteration of smectite due to concrete leachates is restricted to the first millimetres of the bentonite block.

In the three tests, calcite and brucite were identified at the interface. Below them, a continuous layer of a Ca-rich gel phase (presumably portlandite-carbonate composition) was grown. C-S-H gels, such as tobermorite or jennite, were found on the surface of the bentonite block. Ettringite and gypsum were precipitated on the surface of the bentonite block after 12 months of operation.

Analysis of bentonite in contact with concrete confirmed the neoformation of a Mg-trioctahedral smectitic phase. Saponite-like phase was present at the interface, due to the Mg-enrichment of bentonite.

The thickness of bentonite affected by the enrichment in Mg was estimated to be a few millimetres from the interface. In the first 2-3 mm collected from the interface in the 12 and 18-month tests, the increase of the interlayer space in the smectite was observed. These changes could result from the formation of a brucite-saponite-smectite.

Formation of secondary phases could have a clogging effect on bentonite, decreasing the porosity of bentonite at the interface.

4. Geochemical evolution of bentonite

4.1 Chemical Analysis

4.1.1 Cation Exchange Capacity (CEC)

Cation Exchange Capacity (CEC) in bentonite tends to rise as we approach the interface. As a result of C-S-H precipitation, there is a marked increase in the CEC values. The CEC values obtained for unaltered FEBEX

Table XIII. CEC values measured for samples collected from the 6 and 12-month test.

	CEC (meq/100 g)	
Distance from the interface (cm)	**6 months**	**12 months**
0	96,3	96,3
2,4	90,1	90,1
4,8	92,2	86,5
7,2	88	86,4
FEBEX	88,14	

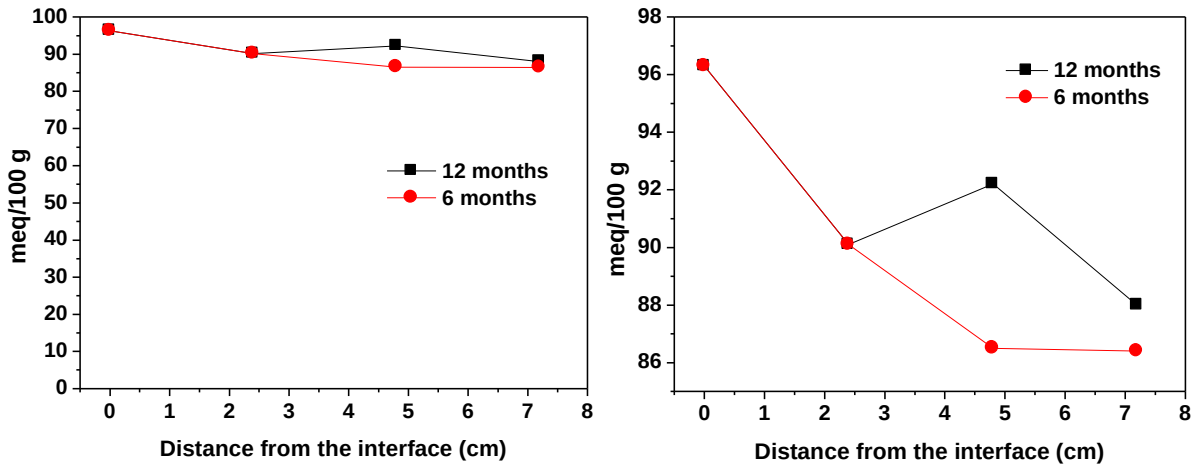

Figure 37. CEC values measured for simples collected from the 6 and 12 month-tests.

4.1.2 Exchangeable cations

Regarding exchangeable cations (Figure 38), Ca^{2+} and K^{+} do not manifest consistent variations along the compacted bentonite block. Nevertheless, an increase of Na^{+} and a drop in Mg^{2+} is observed at the interface. At the interface, Mg^{2+} mobility could be involved in the formation of saponite.

Table XIV. Exchangeable cations (meq/100g) (CsNO3 0.5N, pH 7) measurements in the 6, 12 and 18 month-test.

Exchangeable cations		**meq/100 g**			
Test	**Section**	**Ca**	**Mg**	**Na**	**K**
6 months	*Hydration*	35	17	34	3
	Intermediate	37	25	26	3
	Heating	33	36	21	3
12 months	*Hydration*	42	13	35	3
	Intermediate – upper	41	19	33	3
	Intermediate – lower	44	15	31	3
	Heating	41	31	19	3
18 months	*Interface*	39	23	35	4
	Hydration	47	18	17	4
	Intermediate – upper	44	18	36	4
	Intermediate – lower	43	21	34	3
	Heating	37	50	20	5
FEBEX reference values		40	32	29	3

4.1.3 Soluble extracts (1:8 S/L)

Since most relevant transport processes occurring in the cell may be inferred from the behaviour of conservative species, analysis of anions and cation present in soluble extracts was performed.

Temperature and hydraulic gradients induce the movement of soluble ions towards the heater.

In average, mass balances calculated for each ion show a general increase in the three tests dismantled. Increasing saline contents are a consequence of the highly-saline solution used for hydration (Table II) together with concrete leachates.

Soluble anions

Soluble anions values measured in the aqueous extracts (1:8 S/L) are shown in Table XV. Chloride, sulfate and sodium increased greatly in the section close to the heater.

Chloride distribution is closely related to the thermal gradient (Figure 39). Cl^- is easily dissolved and transported as the water front moves to the unsaturated areas. Leaching, as the saturation front progresses, thermal convection and diffusion are the mechanisms involved in Cl^- mobilization [73]. Chloride is mostly concentrated in areas close to the contact with the heater. Its amount seems to be increasing with test time.

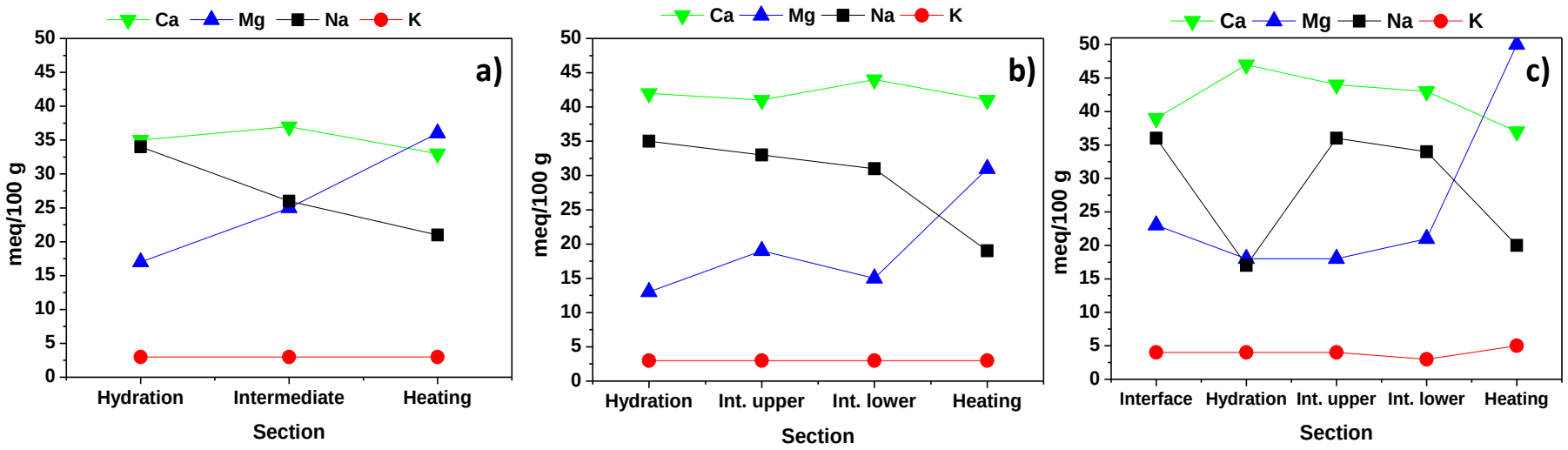

Figure 38. Exchangeable cations measured in the three tests dismantled after: a) 6 ; b) 12 and c) 18 months.

Table XV. Soluble anions concentrations measured in the aqueous extracts (1:8 S/L) for the 6, 12 and 18-month test.

Soluble anions		**mmol soluble anion /100g dry bentonite**		
Test	**Section**	**Cl^-**	**SO_4^{2-}**	**F^-**
6 months	*Hydration*	0.013	0.016	0.087
	Intermediate	0.027	2.041	0.052
	Heating	6.124	0.886	0.046
12 months	*Hydration*	0.139	0.094	0.083
	Intermediate	0.047	0.121	0.048
	Heating	6.225	2.949	0.028
18 months	*Interface*	0.033	0.025	---
	Hydration	0.024	0.022	---
	Intermediate – upper	0.021	0.027	---
	Intermediate – lower	0.018	0.063	---
	Heating	9.266	2.173	---
FEBEX reference values		1.713	0.731	---

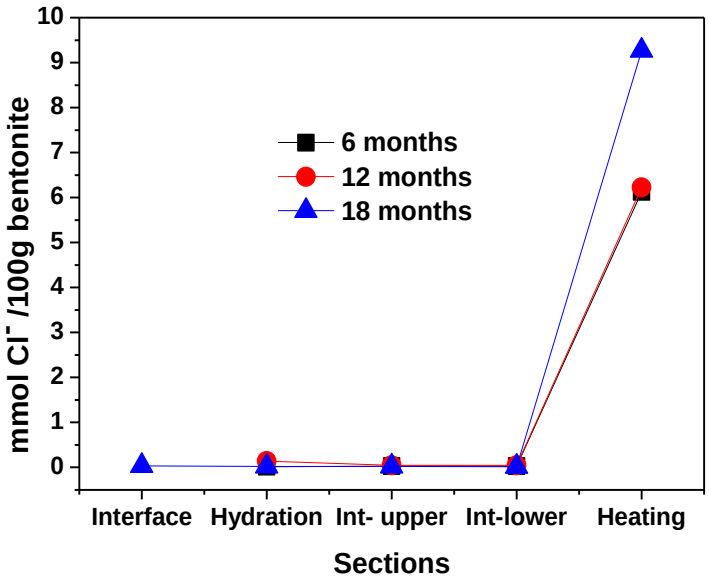

Figure 39. Soluble chloride values obtained from the 6, 12 and 18-month tests.

Transport mechanisms for other chemical species are similar. However, their concentration patterns are more complex, as these species are affected by dissolution/precipitation and ion exchange. Sulfate content reaches its maximum value at the contact with the heater in the case of the 12 and 18-month tests. However, sulfate content in the 18-month test is one third of the value measured for the 12-month test. No explanation has been found for such abnormal behaviour.

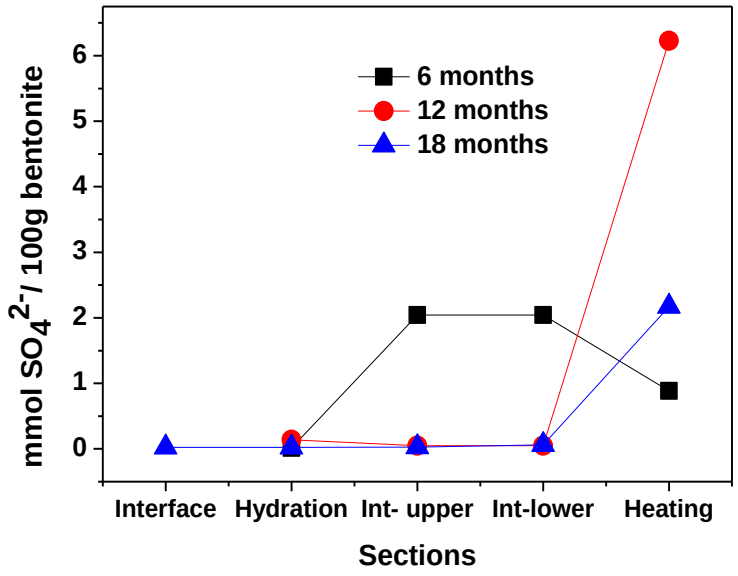

Figure 40. Soluble sulfate values measured in the aqueous extracts from the 6, 12 and 18-month tests.

Soluble cations

Soluble cations values are displayed in Table XVI. The main counterion that followed chloride in all the tests is sodium, decreasing close to the hydration source and increasing towards hotter zones (Figure 41). However, sodium concentration is not only controlled by advective transport but also by cation exchange reactions.

There is an overall increase of magnesium, calcium and potassium along the bentonite block (Table XVI). As in the case of sodium, they are moving towards the heater (Figure 41).

Table XVI. Soluble cations concentrations measured in the aqueous extracts (1:8 S/L) for the 6, 12 and 18-month tests.

Soluble cations		**mmol soluble cations / 100g dry bentonite**			
Test	**Section**	**Ca**	**Mg**	**Na**	**K**
6 months	*Hydration*	0.08	0.00	2.37	0.03
	Intermediate	0.08	0.07	6.43	0.02
	Heating	0.26	0.38	7.51	0.05
12 months	*Hydration*	0.01	0.01	1.51	0.01
	Intermediate	0.01	0.00	1.63	0.02
	Heating	0.71	0.98	9.51	0.18
18 months	*Interface*	0.04	0.04	2.73	0.03
	Hydration	0.02	0.01	2.26	0.02
	Intermediate – upper	0.01	0.03	1.60	0.01
	Intermediate – lower	0.01	0.01	2.21	0.01
	Heating	0.78	0.98	10.75	0.25
FEBEX reference values		0.02	0.07	4.71	0.07

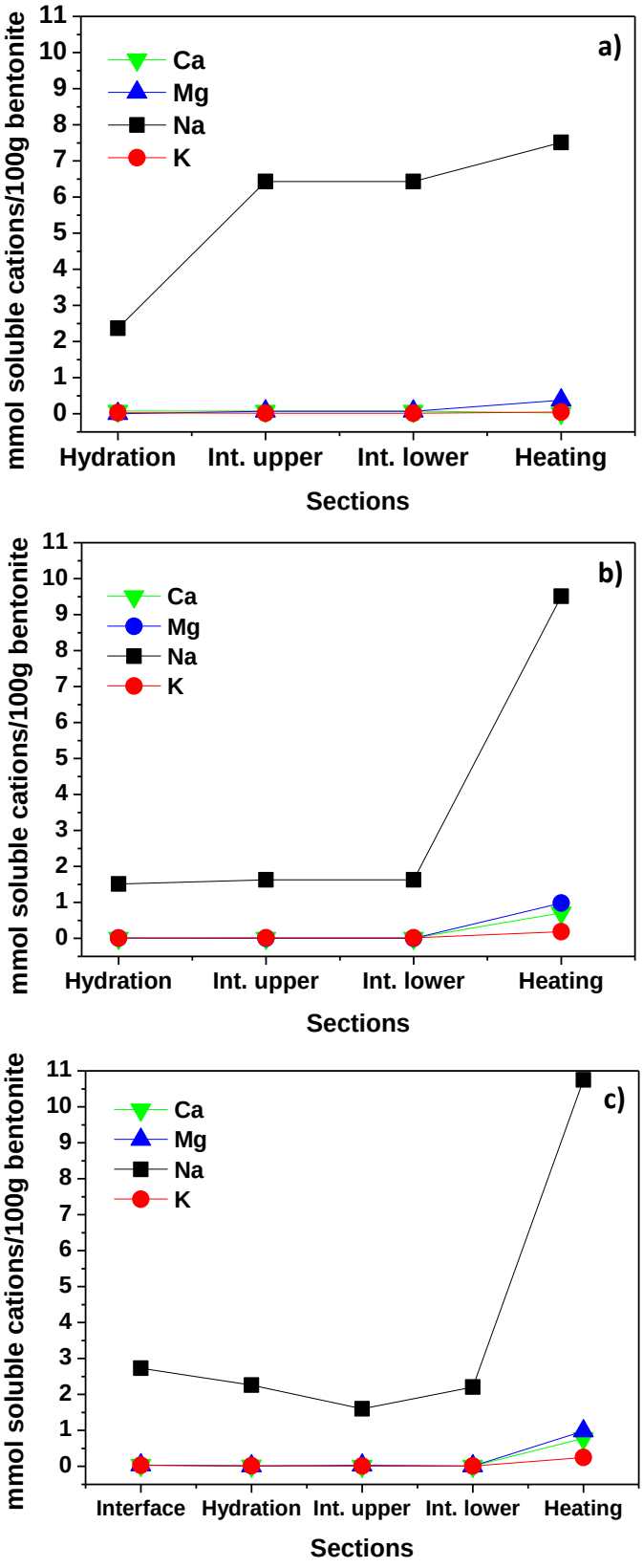

Figure 41. Cations measured in soluble extracts (1:8) from samples collected in the 6, 12 and 18-month tests.

Calcium content increased over time either in the exchange complex or the soluble extracts (Figure 42). Calcium is supplied by concrete leaching.

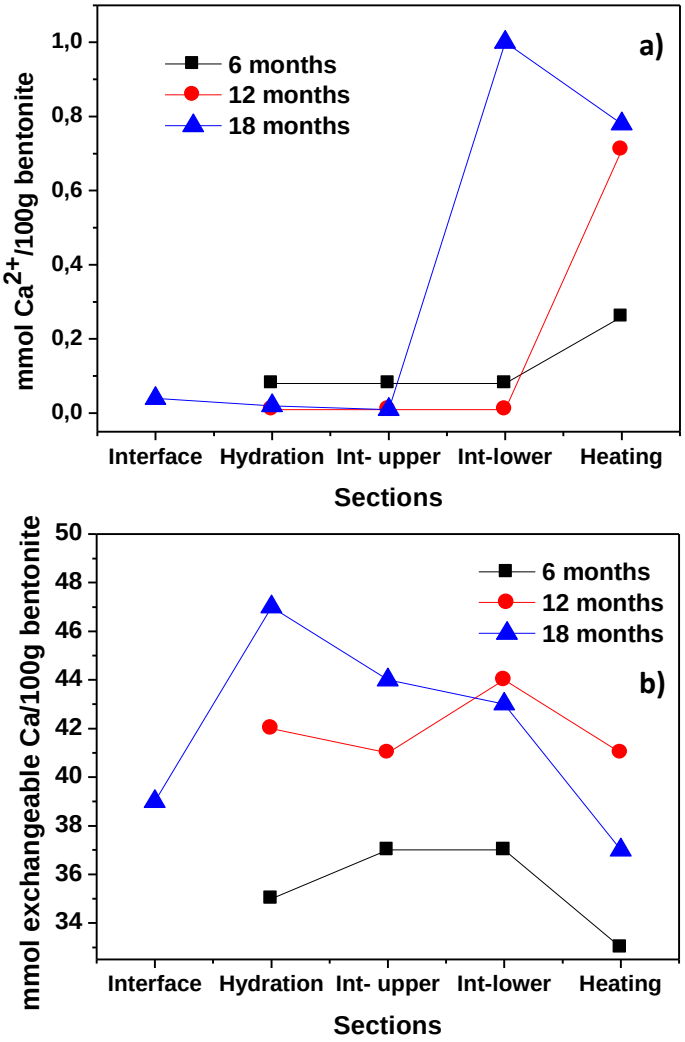

Figure 42. a) Calcium measured in soluble extracts (1:8 S:L); b) Exchangeable calcium values from the 6, 12 and 18-month tests.

4.2 Conclusions

Due to temperature and hydraulic gradients, salt redistribution occurs along the bentonite block. Concrete leaching induces several processes affecting bentonite. As previously discussed, neoformation of smectitic phases, such as saponite, occurs at the interface. Ca-rich gels, calcite, CSH or brucite precipitates were formed as well as the increase of calcium content in the exchange complex and in the soluble extracts.

Besides, concrete leaching induces the increase of calcium near the concrete/bentonite interface. Chloride and sulfate mass balances indicate that the

overall content in the bentonite block has increased due to the highly saline solution used for hydration. Chloride and sulfate tend to concentrate near the heater.

Soluble cations increased slightly, except for Na, whose increase is much more noticeable.

Redistribution of the exchangeable cations occurred due to the thermal gradient. Similar patterns were observed in the three tests dismantled. Na and Mg seem to follow complementary trends. Na increases in saturated areas, whereas Mg increases near the contact with the heater.

5. Conclusions

5.1 General conclusions

This report tries to compile the existing data obtained from the characterization of the three cells dismantled in the framework of NF-Pro Project.

This work will be updated with results collected from the analysis of the cells dismantled after 4.5 and 7 years of operation.

The sequential dismantling of the series of tests assembled during NF-Pro, has allowed obtaining few good tips about the evolution of the concrete-bentonite system.

The conclusions chapter has been divided into three sections, in order to maintain the general structure of this report.

The most remarkable conclusion achieved during the data analysis is the space limited significance of bentonite transformation. Alteration of bentonite occurs locally in the first 2 to 4 mm from the concrete-bentonite interface. Saponite has been identified in the 12 and 18-month tests.

5.2 Concrete

- In the three cells dismantled, sulfate-rich phases, such as gypsum and ettringite, were identified by means of FTIR, XRD and SEM analyses, basically inside the pores near the concrete/bentonite interface.

- Porosity increased with time due to the dissolution of the concrete matrix.

- High concentration of sulfate in the hydrating solution, together with the leaching of salts from the upper areas is responsible for the formation of these new phases close to the interface.

- Decalcification of the concrete surface in contact with hydration occurred, as well as carbonation.

5.3 Concrete – bentonite interface

- In the three tests, calcite and brucite were identified at the interface. Below them, a continuous layer of Ca-rich gels (small precipitates of portlandite-carbonated phases) was grown. C-S-H gels, such as tobermorite or jennite, were found on the surface of the bentonite block. Ettringite and gypsum were precipitated on the surface of the bentonite block after 12 months of operation.

- Analysis of bentonite in contact with concrete confirmed the neoformation of a Mg-trioctahedral smectitic phase. This phase is Saaponite-like and was present at the interface, due to the Mg-enrichment of bentonite.

- The thickness of bentonite affected by the enrichment in Mg was estimated to be a few millimetres from the interface. In the first 2-3 mm collected from the interface in the 12 and 18-month tests, the increase of the interlayer space in the smectite was observed. These changes could result from the formation of a brucite-saponite-smectite.

- Formation of secondary phases could have a clogging effect on bentonite, decreasing the porosity of bentonite at the interface.

5.4 Bentonite

- Due to temperature and hydraulic gradients, salt redistribution occurs along the bentonite block.

- Concrete leaching induces the increase of calcium near the concrete/bentonite interface. Calcium content increased in both, the exchange complex and the soluble extracts.

- Chloride and sulfate mass balances indicate that the overall content in the bentonite block has increased due to the highly saline solution used for hydration. Chloride and sulfate tend to concentrate near the heater.

- Soluble cations increased slightly, except for Na, whose increase is much more noticeable.

- Redistribution of the exchangeable cations occurred due to the thermal gradient. Similar patterns were observed in the three tests dismantled. Na and Mg seem to follow complementary trends. Na increases in saturated areas, whereas Mg increases near the contact with the heater.

6. References

1. Lothenbach, B. and F. Winnefeld, *Thermodynamic modelling of the hydration of Portland cement.* Cem. Concr. Res., 2006. **36**(2): p. 209-226.
2. Damidot, D., et al., *Thermodynamics and cement science.* Cem. Concr. Res., 2011. **41**: p. 679-695.
3. Eberl, D.D., B. Velde, and T. McCormick, *Synthesis of illite-smectite from smectite at earth surface tempeatures and high pH.* Clay Minerals, 1993. **28**: p. 49-60.
4. Bauer, A. and G. Berger, *Kaolinite and smectite dissolution rate in high molar KOH solutions at 35ºC and 80ºC.* Applied Geochemistry, 1998. **33**: p. 906-916.
5. Bauer, A. and B. Velde, *Smectite transformation in high molar KOH solutions.* Clay Minerals, 1999. **34**: p. 259-273.
6. Cuevas, J., et al., *The alkaline reaction of FEBEX bentonite: a Contribution to the study of the performance of bentonite/concrete engineered barrier systems.* Journal of Iberian Geology, 2006. **32**: p. 151-174.
7. Huertas, F., *Effects of cement of clay barrier performance, ECOCLAY project: Final Report*. 2000, European Commission: Brussels.
8. Pusch, R., *Chemical interaction of clay buffer materials and concrete*. 1982, SKB: Stockholm.
9. Pusch, R., et al., *Interaction of cement and smectitic clay - theory and practice.* Applied Clay Science, 2003. **23**: p. 203-210.
10. Anderson, K., et al., *Chemical composition of cement pore waters.* Cement and Concrete Research, 1989. **19**: p. 327-332.
11. Lunden, I. and K. Anderson, *Modelling the mixing of cement pore water and groundwater using the PHREEQC code*, in *Scientific Basis for Nuclear Waste Management - Materials Research Society Symposium Proceedings*. 1989, Materials Research Society: Warrendale, PA. p. 949-956.
12. Jeffries, N.L., C.J. Tweed, and S.J. Wisbey, *The effects of changes in pH in a clay surrounding a cementitious repository*, in *Scientific Basis for Nuclear Waste Management - Material Research Society Symposium Proceedings*. 1988, Materials Research Society: Warrendale, PA. p. 43-52.
13. Haworth, A., S.M. Sharland, and C.J. Tweed, *Modeling of the degradation of cement in a nuclear waste repository*, in *Scientific Basis for Nuclear Waste Management - Materials Research Society Symposium Society*. 1989, Materials Research Society Warrendale, PA. p. 447-454.
14. Berner, U., *A Thermodynamic description of the evolution of porewater chemistry and Uranium Speciation during the degradation of cement.* . 1990, Nagra NTB: Baden, Switzerland.

15. Reardon, E.J., *An ion interaction model for the determination of chemical equilibrium in cement/water systems.* Cement and Concrete Research, 1990. **20**: p. 175-192.

16. Viellard, P. and F. Rassineux, *Thermodynamic and geochemical modelling of the alteration of two cement matrices.* Applied Geochemistry, 1992. **1**: p. 125-136.

17. Mohnot, S.M., J.H. Bae, and W.L. Foley, *A study of alkali/mineral reactions*, in *SPE Reservoir Engineering*. 1987. p. 653-663.

18. Carroll-Webb, S.A. and J.V. Walther, *A surface complex reaction model for the pH-dependence of corundum and kaolinite dissolution.* Geochimica et Cosmochimica Acta, 1988. **52**: p. 2609-2623.

19. Carroll, S.A. and J.V. Walther, *Kaolinite dissolution at 25, 60 and 80ºC.* American Journal of Science, 1990. **280**: p. 797-810.

20. Chermak, J.A., *Low temperature experimental investigation of the effect of high pH NaOH solutions of the Opalinus shale, Switzerland.* Clays and Clay Minerals, 1992. **41**: p. 365-372.

21. Huang, W.L., *The formation of illitic clays from kaolinite in KOH solution from 225 to 350ºC* Clays and Clay Minerals, 1993. **41**: p. 645-654.

22. Bauer, A., B. Velde, and G. Berger, *Kaolinite transformation in high molar KOH solutions.* Applied Geochemistry, 1998. **13**: p. 619-629.

23. Cama, J., et al., *Smectite dissolution kinetics at 80 degrees and pH 8.8.* Geochimica et Cosmochimica Acta, 2000. **64**: p. 2701-2717.

24. Taubald, H., et al., *Experimental investigation of the effect of high-pH solutions on the Opalinus Shale and the Hammerschmiede Smectite.* Clay Minerals, 2000. **35**: p. 515-524.

25. Huertas, F.J., et al., *Kinetics of montmorillonite dissolution in granitic solutions.* Applied Geochemistry, 2001. **16**: p. 397-407.

26. Bouchet, A. and F. Rassineux, *Echantillons d'Argiles du Forage EST 104: Étude minéralogique Approfondie*. 1997, Andra: Chatenay-Malabry, France. p. 107.

27. Claret, F., *Caractérisation structurale des transitions minéralogiques dans les formations argileuses: Contrôles et implications géochimiques des processus dillitisation. Cas particulier d'une perturbation alkaline dans le Callovo-Oxfordien Laboratoire souterrain Meuse-Haute-Marne*. 2001, Université Joseph Fourier: Grenoble, France. p. 174.

28. Rassineux, F., et al., *Expandability-layer stacking relationship during experimental alteration of a Wyoming bentonite in pH 13.5 solutions at 25 and 60ºC.* Clay Minerals, 2001. **36**: p. 197-210.

29. Nakayama, S., et al., *Dissolution of montmorillonite in compacted bentonite by highly alkaline aqueous solutions and diffusivity of hydroxide ions.* Appl. Clay Sci., 2004. **27**: p. 53-65.

30. Fernández, R., et al., *Reactivity of the cement-bentonite interface with alkaline solutions using transport cells.* Appl Geochem, 2006. **21**: p. 977-992.

31. Fernández, R., et al., *Precipitation of chlorite-like structures during OPC porewater diffusion through compacted bentonite at 90ºC.* Appl. Clay Sci., 2013. **83-84**: p. 357-367.

32. Fernández, R., et al. *The stability of zeolites and C-S-H in the high pH reaction of bentonite*. in *Cementitious Materials in Safety Cases for Geological Repositories for Radioactive Waste: Role, Evolution and Interactions*. 2012. Brussels, Belgium: NEA.

33. ENRESA, *Full-Scale Engineered Barriers Experiment in Crystalline Host Rock. Bentonite: Origin, Properties and Fabrication of Blocks.* . 1998, ENRESA.

34. Villar, M.V., *Thermo-hydro-mechanical characterization of a bentonite from Cabo de Gata. A study applied to the use of bentonite as sealing material in high level radioactive waste repositories*. 2002, ENRESA: Madrid.

35. Hidalgo, A., et al., *Microstructural characterization of leaching effects in cement pastes due to neutralization of their alkaline nature. Part I: portland cement pastes.* Cement and Concrete Research, 2007. **37**: p. 63-70.

36. Meier, L.P. and G. Kahr, *Determination of the cation exchange capacity (CEC) of clay minerals using the complexes of copper(II) ion with triethylenetetramine and tetraethylenepentamine.* Clays and Clay Minerals, 1999. **47**(3): p. 386-388.

37. Shawhney, B.L., *Potassium and Cesium ion selectivity in relation to clay mineral microstructure.* Clay and Clay Minerals, 1970. **18**: p. 47-52.

38. Taylor, H.F.W., *Cement Chemistry*. 1990, New York: Academic Press.

39. Xu, A. and D. Viehland, *Observation of a mesostructure in calcium silicate hydrate gels of portland cement.* Physical Review Letters, 1996. **77**: p. 952-955.

40. Flint, E.P. and L.S. Wells, *Study of the system CaO-SiO_2-H_2O at 30º and the reaction of water on the anhydrous calcium silicates.* Journal of Research of the National Bureau Standards, 1934. **12**: p. 751-783.

41. Roller, P.S. and J.G. Ewin, *The system calcium oxide-silica-water at 30ºC. The association of silicate in dilute alkaline solution.* Journal of the American Chemical Society, 1940. **62**: p. 461.

42. Taylor, H.F.W., *Hydrated calcium silicates. Part I, compound formation at ordinary temperatures.* Journal of the American Chemical Society, 1950. **275**: p. 3682-3690.

43. Greenberg, S.A., T.N. Chang, and E. Anderson, *Investigation of Colloidal Hydrated Calcium Silicates I. Solubility relationships in the calcium oxide-silica-water system at 25ºC.* Journal of Physical Chemistry, 1965. **64**: p. 1151-1157.

44. Greenberg, S.A. and T.N. Chang, *Investigation of Colloidal Hydrated Calcium Silicates II. Solubility relationships in the calcium oxide-silica-water system at 25ºC.* Journal of Physical Chemistry, 1965. **69**: p. 182-188.

45. Fujii, K. and W. Kondo, *Heterogeneous equilibrium of calcium silicate hydrate in water at 30ºC.* Journal of the Chemical Society Dalton Transitions 1981. **2**: p. 645-651.

46. Glasser, F.P., E.E. Lachowski, and D.E. Mcphee, *Compositional model for calcium silicate hydrate (C-S-H) gels, their solubilities, and fee energies of formation.* Journal of the American Chemical Society, 1987. **70**: p. 481-485.

47. Hamid, S.A., *The crystal structure of 11A natural tobermorite* $Ca_{2.25}[Si_3O_{7.5}(OH)_{1.5}]\cdot 1H_2O$. Z. Kristallogr., 1981. **154**: p. 189-198.

48. Merlino, S., E. Bonaccorsi, and T. Armbruster, *Tobermorites: their real structure and order-disorder (OD) character* American Mineralogist, 1999. **84**: p. 1613-1621.

49. Cong, X. and R.J. Kirkpatrick, *MAS NMR study of the structure of calcium silica hydrate.* Advanced Cement Based Materials, 1996. **3**: p. 144-156.

50. Klur, I., *Étude par RMN de la structure des silicates de calcium hydratés*. 1996, Université Paris 06: Paris.

51. Klur, I., et al., *CSH structure evolution with calcium content by multinuclear NMR*, in *Nuclear Magnetic Resonance Spectroscopy of Cement-Based Materials*, P. Colombet, et al., Editors. 1998, Springer: Berlin. p. 119-141.

52. Shaw, S., S.M. Clark, and C.M.B. Henderson, *Hydrothermal formation of the calcium silicate hydrates, tobermorite* ($Ca_5Si_6O_{16}(OH)_2\cdot 4H_2O$) *and xonotlite* ($Ca_6Si_6O_{17}(OH)_2$)*: an in situ synchrotron study.* Chemical Geology, 2000. **167**: p. 129-140.

53. Rodger, S.A., et al., *Hydration of tricalcium silicate followed by silicon-29 NMR with cross-polarization.* Journal of the American Ceramic Society, 1988. **71**: p. 119-141.

54. Grutzeck, M., A. Benesi, and B. Fanning, *Silicon-29 magic angle spinning nuclear magnetic resonance study of calcium silicate hydrates.* Journal of the American Ceramic Society, 1989. **71**: p. 91-96.

55. Faucon, P., J.M. Delaye, and J. Virlet, *Molecular dinamics simulation of the structure of calcium silicate hydrates I.* $Ca_{4+x}Si_6O_{14+2x}(OH)_{4-2x}(H_2O)_2$ $(0<x<1)$. Journal of Solid State Chemistry, 1996. **127**: p. 92-97.

56. Thomas, J.J., et al., *Effects of decalcification on the microstructure and surface area of cement and tricalcium silicate pastes.* Cement Concrete Research, 2004. **34**(12): p. 2297-2307.

57. Harris, A.W., et al., *Testing of models of dissolution of cements-leaching of synthetic C-S-H gels.* Cement and Concrete Research, 2002. **32**: p. 731-746.

58. de la Cruz, B., et al., *WP 2-1: Critical review and incorporation of information of E.C., national and international programmes in RTD component 2*, in *European Commission Report*. 2004, European Commision: Brussels, Belgium.

59. Andrade, C., et al., *Some principles of service life calculation of reinforcements and in situ corrosion monitoring by sensors in the radioactive waste containers of El Cabril disposal (Spain).* Journal of Nuclear Materials 2006. **358**: p. 82-95.

60. Biscontin, G., M. Pellizon Birelli, and E. Zendri, *Characterization of binders employed in the manufacture of Venetian historical mortars.* Journal of Cultural Heritage, 2002. **3**: p. 31-37.

61. Torres, S.M., et al., *Long-term durability of Portland-limestone ceent mortars exponed to magnesium sulfate attack.* Cement and Concrete Composites, 2003. **25**: p. 947-954.

62. Xu, P., et al., *Structure of calcium silicate hydrate (C-S-H): near-, mid-, and far-infrared spectroscopy.* Journal of the American Ceramic Society, 1999. **82** (3): p. 742-748.

63. Farmer, V.C., *The Infrared Spectra of Minerals*. 1974, London: Mineralogical Society.

64. Gollop, R.S. and H.F.W. Taylor, *Microstructural and microanalytical studies of sulfate attack: III. Sufate resistant Portland cement: Reaction with sodium and magnesium sulfate solution.* Cement and Concrete Research, 1995. **25**(7): p. 1581-1590.

65. Gollop, R.S. and H.F.W. Taylor, *Microstructural and microanalytical studies of sulfate attack: I. Ordinary Portland cement paste.* Cement and Concrete Research, 1992. **22**(6): p. 1027-1038.

66. González, M.A. and E.F. Irassar, *Ettringite formation in low C_3A Portland cement exposed to sodium sulfate solution.* Cement and Concrete Research, 1997. **27**(7): p. 1061-1072.

67. Mehta, P.K., *Mechanism of sulfate attack on Portland cemnt concrete - another look.* Cement and Concrete Research, 1983. **13**(3): p. 401-406.

68. Irassar, E.F., V.L. Bonavetti, and M. González, *Microstructural study of sulfate attack on ordinary and limestone Portland cements at ambient temperature.* Cement and Concrete Research, 2003. **33**: p. 31-41.

69. Rasheeduzzafar, R., *Influence of cement composition on concrete durability.* ACI Materials Journal, 1992. **89**(6): p. 574-586.

70. Diamond, S., *Microscopic features of groundwater induced sulfate attack in highly permeably concretes*, in *Fifth CANMET/ACI International Conference on Durability of Concrete*, V.M. Malhotra, Editor. 2000, American Concrete Institute: Barcelona, Spain. p. 403-416.

71. Collepardi, M., *Thaumasite formation and deterioration in historic buildings.* Cement and Concrete Composites, 1999. **21**(2): p. 147-154.

72. Richardson, I.G., C.R. Wilding, and M.J. Dickson, *The hydration of blastfurnace slag cements.* Advances in Cement Research, 1989. **2**: p. 147-157.

73. Villar, M.V., J. Cuevas, and P.L. Martín, *Effects of heat/waterflow interaction on compacted bentonite.* Engineering Geology, 1996. **41**: p. 257-267.